Desmosome dualism: most of the junction is stable but a plakophilin moiety is persistently dynamic

Judith B Fülle[1,2], Henri Huppert[1,3], David Liebl[4], Jaron Liu[3], Rogerio Alves de Almeida[1], Bian Yanes[1], Graham D Wright[2,4], E Birgitte Lane[2]*, David R Garrod[1]*, Christoph Ballestrem[1]*

[1] Wellcome Trust Centre for Cell-Matrix Research, University of Manchester, Manchester M13 9PT, UK.
[2] Skin Research Institute of Singapore, Agency of Science Technology and Research (A*STAR), 8A Biomedical Grove, #06-06 Immunos, 138648 Singapore, Singapore.
[3] Institute of Medical Biology, Agency of Science Technology and Research (A*STAR), 61 Biopolis Dr, 138673 Singapore, Singapore.
[4] A*STAR Microscopy Platform, Research Support Centre, Agency of Science Technology and Research (A*STAR), Biopolis 138673, Singapore, Singapore.

Correspondence and requests for material should be addressed to
Christoph Ballestrem: christoph.ballestrem@manchester.ac.uk
David Garrod: d.garrod@manchester.ac.uk
E Birgitte Lane: birgit.lane@sris.a-star.edu.sg
* This work was a collaboration between the research groups of EB Lane, DR Garrod and C Ballestrem

Keywords: Desmosome, Adhesion, Plakophilin

Summary statement:
Desmosomes consist of a stable and a dynamic signalling moiety. The dualistic composition is maintained during adhesion maturation and internalisation of whole desmosomes during cell scattering.

Abstract

Desmosomes, strong cell-cell junctions of epithelia and cardiac muscle, link intermediate filaments to cell membranes and mechanically integrate cells across tissues, dissipating mechanical stress. They comprise five major protein classes – desmocollins and desmogleins (the desmosomal cadherins), plakoglobin, plakophilins and desmoplakin - whose individual contribution to the structure and turnover of desmosomes is poorly understood. Using live-cell imaging together with FRAP and FLAP we show that desmosomes consist of two contrasting protein moieties or modules: a very stable moiety of desmosomal cadherins, desmoplakin and plakoglobin, and a highly mobile plakophilin

(Pkp2a). As desmosomes mature from calcium-dependence to calcium-independent hyper-adhesion, their stability increases, but Pkp2a remains highly mobile. We show that desmosome down-regulation during growth-factor-induced cell scattering proceeds by internalisation of whole desmosomes, which still retain a stable moiety and highly mobile Pkp2a. This molecular mobility of Pkp2a suggests a transient and probably regulatory role for Pkp2a in desmosomes.

Introduction

Vertebrates have evolved several multimolecular systems to provide the cell cohesion and resilience necessary to withstand mechanical stress and deformation without a protective exoskeleton. Epithelia, the functional interfaces around, within and between body organs, have evolved complex multiprotein desmosome cell-cell junctions. Desmosomes connect to cytoplasmic intermediate filament networks to form a mechanically resilient trans-cellular tissue system. Together with adherens junctions and tight junctions, desmosomes enable integration and stratification of epithelia, whilst ensuring that barrier function is maintained at all times and also that damaged tissue cells can be replaced. Loss of desmosome function is linked to severe diseases, particularly in mechanically challenged tissues such as skin and cardiac muscle (reviewed by (Chidgey and Dawson, 2007; Delmar and McKenna, 2010; Dusek and Attardi, 2011; Ishida-Yamamoto and Igawa, 2014; Maruthappu et al., 2019; Spindler et al., 2018; Thomason et al., 2012).

Within the desmosomal macromolecular complex, the extracellular domains of the desmosomal cadherins (DCs), desmocollins (Dsc) and desmogleins (Dsg), bind tightly to their counterparts on the adjacent cells, while their intracellular domains connect via plakoglobin (PG) and plakophilins (Pkps) to intermediate filament–binding dimers of desmoplakin (DP) (Garrod and Chidgey, 2008; Green et al., 2019). Desmosomes of intact homeostatic tissues exist in a state of hyper-adhesion, rendering them particularly stress-resistant (Wallis et al., 2000; Garrod et al., 2005). Whilst newly formed desmosomes need extracellular calcium for adhesion through their DCs, mature hyper-adhesive desmosomes remain robustly attached to each other even after experimental removal of extracellular calcium by experimental chelation of calcium ions (Ca^{2+}).

Hyper-adhesion is developmentally regulated in the mouse embryo and is acquired with time in confluent culture of several cell lines (Kimura et al., 2007; Kimura et al., 2012; Wallis et al., 2000). It has been suggested that hyper-adhesion is associated with an ordered arrangement of the extracellular domains of the desmosomal cadherins, indicated by the presence of an electron-dense midline present halfway between the desmosomal cell membranes, and that this may result in Ca^{2+} being locked into the structure (Garrod et al., 2005). It has been reported that this ordered arrangement of extracellular domains of genetically modified Dsg3 is lost upon removal of extracellular Ca^{2+}, both from pharmacologically-induced hyper-adhesive and calcium-dependent desmosomes, suggesting the ordering of DCs is not the only factor involved in desmosomal adhesion (Bartle et al., 2020; Bartle et al., 2017).

Whilst tissue integrity depends upon the maintenance of stable cell-cell junctions, cells must retain the ability to free themselves from their neighbours in order to move or to get rid of damaged cells. During embryonic development, in wound healing and tissue regeneration, cell adhesion must be temporarily relaxed or lost for cells to undertake tissue remodelling. This is seen in epithelial-to-mesenchymal transition (EMT), the conversion of compact epithelial sheets to solitary or small groups of motile cells, which occurs during development and in metastatic progression of some cancers, and is often triggered by growth factor signalling (Nieto et al., 2016).

Despite the importance of cell adhesion in health and disease, little is known about how desmosomal adhesion is lost *in vivo*. A limited amount of evidence suggests that loss of desmosome-dependent cell adhesion may occur through internalisation of whole desmosomes by the cells involved (Allen and Potten, 1975; Garrod et al., 2005). This has not been studied in detail because no tissue culture model of the process exists. Studies on the internalisation of half desmosomes, induced by (non-physiological) Ca^{2+} chelation, have shown that this process is actin dependent, that the internalised half-desmosomes remain intact until degraded by a combination of lysosomal and proteasomal activity, and that desmosomal proteins were not recycled (McHarg et al., 2014). Whether similar mechanisms apply to the internalisation of whole desmosomes under physiological conditions remains to be determined.

Desmosomes are undoubtedly highly stable structures, stability being key to their function, and it is becoming clear that the protein exchange rates within desmosomes mirror their stability as has been shown for Dsg2, Dsg3, Dsc2, DP and PG (Bartle et al., 2020; Foote et al., 2013; Gloushankova et al., 2003; Lowndes et al., 2014; Moch et al., 2019; Vielmuth et al., 2018; Windoffer et al., 2002). Nevertheless they are also dynamic, with a life cycle of four phases: *de novo* assembly from their component molecules, a weakly-adhesive calcium-dependent phase compatible with cell migration, a strongly adhesive calcium-independent phase in tissue homeostasis, and desmosome removal or breakdown as epithelia become activated by relevant signalling.

We investigated the complex relationships between desmosomal proteins during the last three stages of this life cycle using time-lapse fluorescence microscopy including fluorescence recovery after photobleaching (FRAP) and fluorescence loss and localisation after photoactivation (FLAP). A culture model for desmosome internalisation was established to mimic the *in vivo* situation more closely, and we observed that one of the desmosomal proteins, plakophilin 2a (Pkp2a), behaves very differently from the others both in Madin-Darby canine kidney (MDCK) and human colorectal adenocarcinoma (CaCo-2) cells. In calcium-dependent desmosomes the molecular mobility of Dsc2a, Dsg2, PG and DP is very low and is further reduced as the cells become hyper-adhesive, forming a stable desmosomal moiety or module. DP in MDCK cells is mobile initially but stabilises with the stable moiety with the onset of hyper-adhesion. In contrast, Pkp2a shows a unique and persistently dynamic exchange between its desmosomal and cytoplasmic pool. Similar relative protein dynamics persist

when whole desmosomes are internalised during HGF-induced scattering of MDCK cells. These results suggest a uniquely dynamic role for Pkp in desmosomes.

Results

Calcium-dependent desmosomes exhibit differential protein dynamics

To shed light on the behaviour of the individual desmosomal components, we first analysed their dynamic properties using FRAP. The relative mobility of the proteins was assessed by determining their half-time of fluorescence recovery ($t_{1/2}$) and mobile fraction (F_m) (Carisey et al., 2011). Dsc2a, Dsg2, PG, DP and Pkp2a tagged with either neonGreen or eGFP fluorophores were stably expressed in the simple epithelial cell line MDCK type II (Fig. 1 A), a well-established model for the study of cell-cell junctions (Dukes et al., 2011). The cells were plated at confluent density and cultured for 24h prior to FRAP, at which time the majority of the desmosomes showed calcium-dependent adhesion (Fig. S1 A, B) (Wallis et al., 2000).

A wide distribution in the F_m of the desmosome proteins in MDCK cells was observed (Fig. 1 B, Table S1). The transmembrane proteins Dsg2 (F_m=29.8%) and Dsc2a (F_m=35.7%) showed the lowest mobile fractions, closely followed by the cytoplasmic plaque protein PG (F_m=37.7%). DP was slightly more mobile (F_m=50.2%), while Pkp2a showed the highest mobile fraction (F_m=74.6%) (Fig.1C). Analysis of the recovery times showed similar results, with slower recovery times of DCs (Dsg2 $t_{1/2}$=75.7s, Dsc2a $t_{1/2}$=62.9s) and PG ($t_{1/2}$=60.1s) in comparison to the significantly faster one for Pkp2a ($t_{1/2}$=30.1s) (Table S1). To put the high stability of the DCs into perspective against actin-associated cell-cell junction proteins, we measured the mobility of E-cadherin, the adhesion receptor of adherens junctions. Mobile fraction of E-cadherin tagged with mEmerald (E-Cad) was much higher (F_m=52.8%) than the mobile fractions of the DCs, demonstrating that desmosomal receptors are more stable at the cell-cell interface than E-cadherin in adherens junctions (Fig. 1 C, Table S1).

The very low mobile fraction of Dsg2, Dsc2a and PG prompted us to evaluate the contribution of the reversible photobleaching properties of the fluorophores, which can be up to 20% of the fluorescence intensity prior to the bleaching event (Sinnecker et al., 2005). Performing FRAP on paraformaldehyde fixed cells we recorded a F_m=6.8% and $t_{1/2}$=11.3s for neonGreen and a F_m=10.2% and $t_{1/2}$=13.1s for eGFP after 5 minutes of recordings, which readings are related to the inherent recovery properties of the fluorescent tags (reversible photobleaching; red dotted line Fig. 1 B). These recovery rates suggested an even lower mobile fraction of the desmosomal proteins and impaired the determination of accurate $t_{1/2}$ in particular of the stable desmosomal proteins (indicated in Table S1). However, these values cannot directly be subtracted from the F_m and adjusted to $t_{1/2}$ measured in the live cell recordings as the fixation process may lead to conformational changes in the fluorophores that may result in varied lifetimes and properties (Becker, 2012).

To bypass the potential issue of reversible photobleaching and for further analysis, we analysed FLAP (Fig. 2 A). This allowed us to calculate the fluorescence decay within the activated region of interest (ROI) as well as to track the activated fluorescent proteins within their environment. Using photoactivatable-GFP (PaGFP) tagged Dsc2a, with mScarlet-Pkp2a used as a desmosome marker, and PG-PaGFP with Dsc2a-mScarlet, FLAP showed similar protein turnover readings to those found by FRAP. Both techniques showed a low mobile fraction while PaGFP-Pkp2a with Dsc2a-mScarlet as a desmosome marker had a significantly higher turnover as seen by FRAP (Fig. 1 C, 2 B).

These results were recapitulated in transiently transfected human colorectal adenocarcinoma cells (CaCo-2) (Fig. S1 E-H). In both FRAP and FLAP experiments Pkp2a showed a significantly higher mobile fraction of 72.8% and 79.3% respectively in comparison to Dsc2a, PG and DP. Interestingly, DP was less mobile in CaCo-2 cells with a mobile fraction of 24.1% close to those of Dsc2a (24.1%) and PG (21.3%) and to the recently reported mobile fraction of DP of 28% in transiently transfected HaCaT cells (Bartle et al., 2020), indicating that the mobile fraction of DP may vary between cell types and different adhesion states of desmosome in these cell lines.

We conclude that in calcium-dependent desmosomes, DCs and PG form a stable moiety of desmosomes, whereas Pkp2a has a dramatically higher mobile fraction that suggests a more transient association of this protein with desmosomes. In calcium-dependent desmosomes of MDCK cells the mobile fraction of DP is intermediate between that of the stable moiety and the highly mobile Pkp2a.

Plakophilin 2a shows rapid exchange between desmosomes and a cytoplasmic pool

The mobility of desmosomal proteins could be due to either a local exchange of proteins at the plasma membrane or due to an exchange with intracellular pools, or both. In order to determine the mechanism of Pkp2a exchange at desmosomes, we performed further FLAP experiments with MDCK cells. FLAP recordings of Dsc2a-PaGFP activated at the plasma membrane were taken over 30 mins, which confirmed the extraordinarily stable localisation and no apparent lateral diffusion of Dsc2a (Fig. 2 C). In contrast, photoactivated PaGFP-Pkp2a at the same settings distributed rapidly along the entire membrane (Fig. 2 C). To assay the flux between the cytoplasmic pool of Pkp2a and the desmosome-associated Pkp2a, we performed FLAP by targeting the 405nm laser light to a 10 µm diameter circular region of the cytoplasm for localized photoactivation and tracking of PaGFP-Pkp2a out from this region (Fig. 2 D). PaGFP-Pkp2a diffused within seconds throughout the entire cytoplasm and was found to become rapidly enriched at the membrane (Fig. 2 D, E). Line profile analysis revealed overlapping fluorescence intensity peaks of PaGFP-Pkp2a and Dsc2a-mScarlet, indicating the recruitment of Pkp2a from the cytoplasm to desmosomes (Fig. 2 F). Similar FLAP attempts with the other desmosomal components of Dsc2a and PG failed because of their extremely low presence in the cytoplasm (Fig. S1 C). Taken together, the results revealed a previously unknown property of Pkp2a, i.e. that it circulates continuously between the desmosomal plaque and the cytoplasm, in stark contrast to the more stable association of the other studied components with the desmosomes.

Hyper-adhesive desmosomes are more stable yet retain high Pkp2a turnover

We next asked whether the dynamics of the major desmosomal proteins changed as desmosomes matured from calcium-dependent to calcium-independent hyper-adhesion, with two major questions in mind: (a) do the major proteins acquire greater stability, and (b) does Pkp2a remain more dynamic than the other proteins? We first established in all the MDCK cell lines we tested that most desmosomes had become hyper-adhesive after 3 days of confluent culture (Fig. S1 A, B). To investigate whether the adhesive state of desmosomes affects their protein dynamics, we performed FRAP in 3-day confluent MDCK cells (Fig. 3 A, B) and compared them with those obtained in the 1-day cultures (Fig. 1). All the tested desmosomal proteins became significantly less mobile as desmosomes matured to hyper-adhesion (Fig. 3 B, Table S1). In contrast, the mobile fraction of E-cadherin was not significantly reduced over the same time period. Dsg2 showed the lowest mobile fraction of 13.6% followed by Dsc2a and PG (both <25%). Taking into account reversible photobleaching of up to 10% showed that these three proteins remained almost static in cell-cell junctions. The low mobile fraction rendered it impossible to determine a reliable $t_{1/2}$ for the proteins due to potential interference from rapidly reversible photobleaching seen in fixed cells (neonGreen $t_{1/2}$=11.3s, EGFP $t_{1/2}$=13.1s) (Table S1).

A significant decrease of the mobile fractions was also observed for DP and Pkp2a (Fig. 3 C and Table S1). DP showed the greatest decrease in its mobile fraction from 50.2% to 30.0% concomitant with a reduction in the $t_{1/2}$. Although Pkp2a also showed decreased mobile fraction under hyper-adhesive conditions, it retained a high F_m of 58.8%. This was at least twice the level of mobile fractions of the other desmosomal proteins and was particularly striking when line profiles of the bleached regions were compared (Fig. 3 A). These results were confirmed by FLAP (Fig. 3 D, S1 D). The mobile fraction of both Dsc2a and PG tagged with PaGFP was significantly reduced after 3 days of confluent culture but Pkp2a retained a considerably higher turnover.

These results demonstrate a substantial decrease in mobility of the desmosomal components accompanying maturation to hyper-adhesion. Furthermore, they support the idea of a stable desmosomal moiety in which DP joins this module formed by DCs and PG at earlier stages in MDCK cells. Pkp2a, however, has a novel and surprisingly dynamic role.

Intact desmosomes are internalised during cell scattering

The existence of a stable moiety of core desmosomal components, even where the binding of the DCs was calcium-dependent, led us to question whether this would be maintained during desmosome down-regulation, which is required for morphogenesis, wound healing, tissue remodelling and EMT. Alternatively, would desmosomal components become highly mobile leading to desmosome dissolution? In order to create a culture model of desmosome down-regulation that did not require Ca^{2+} chelation, we used HGF-induced scattering of MDCK cells, which leads to phenotypic changes resembling partial EMT, including increased cell motility and loss of cell-cell adhesion (Balkovetz, 1998; Ridley et al., 1995).

Desmosomes were tracked using real-time imaging of mixed populations of MDCK cells expressing either Dsc2a-YFP or Dsg2-mCherry. Thus, where two differentially-labelled cells were in contact, desmosomes were labelled with Dsc2a-YFP (green) on one side and Dsg-mCherry (magenta) on the other (Fig. 4 A, B). To test the validity of this system we first treated such mixed populations with Ca^{2+} chelation, which has been well documented to induce splitting of desmosomal adhesion and internalisation of half desmosomes. Imaging showed the extracellular separation of the desmosomes into two half-desmosomes which were subsequently internalised by their own cell as indicated by the entry of solely magenta or solely green particles into the cells (Fig. 4 A, C). These observations were consistent with the results of previous Ca^{2+} chelation experiments in which half-desmosomes were seen to be internalised (Mattey and Garrod, 1986; McHarg et al., 2014).

In order to monitor the down-regulation of desmosomes in the presence of a physiological calcium concentration, such mixed cell populations were grown on fibronectin-coated glass and induced to scatter by treatment with HGF following serum starvation. Under these conditions, cells growing in small islets started spreading and single cells detached from their neighbours (Fig. S2 A). Treatment with HGF for 6 hours resulted in a significantly greater number of intracytoplasmic desmosome particles (52.2 ± 4.1 cytoplasmic desmosomes/cell) in comparison to untreated cells (1.9 ± 0.3 cytoplasmic desmosomes/cell) (Fig. S2 B). Clustering of internalised desmosomes was observed (Fig. S2 A) so that the number of internalised desmosomes is likely to be an underestimate. High magnification fluorescence imaging at 5-second intervals revealed that desmosomes remained stable at the sites where cells maintained contact. Surprisingly, during the final stages of cell separation, whole desmosomes were rapidly internalised by one or other of the pair of adjacent cells (Fig. 4 B, C, Movie 1), with the entire desmosomal structure becoming engulfed, including cytoplasmic fragments from both cells (i.e. fluorescence signals of Dsc2a-YFP and Dsg2-mCherry). There was no preference for whether the Dsc2a-YFP or the Dsg2-mCherry expressing cell internalised the whole desmosomes (Fig. 4 D). Quantification of the co-localisation of fluorescent particles after internalisation revealed that concomitant internalisation of the Dsg and Dsc complex from opposing cells was the dominant mode of internalisation following HGF treatment (Fig. 4 C). Immunostaining of unpermeablised HGF-treated cells with an antibody specific for the extracellular domain of Dsc2/3 failed to detect internalised desmosome indicating that they were fully internalised and no longer had continuity with the cell surface (Fig. S2 C, D). These results implied that HGF-induced scattering led to the internalisation of whole desmosomes, rather than separation of the desmosomal adhesion receptors of neighbouring cells or the complete dissolution of desmosomes.

To confirm this hypothesis, we performed electron microscopy (EM). We used correlative light and electron microscopy (CLEM) to identify cells with internalised desmosomes (Fig. S2 E). Subsequent ultrastructural analysis of the EM micrographs showed that the internalised, double-labelled structures were indeed morphologically intact desmosomes with attached keratin filaments and remains of the plasma membrane (Fig. 4 G). Comparing the width of desmosome plaques as a readout for their intactness showed only a slight reduction from those of intact desmosomes at the membrane (Fig. 4

F). The great majority (>90%) of desmosomes internalised following HGF treatment were internalised whole, with a small number of structures identified as half-desmosomes (Fig. 4 E, S2 F). We concluded that desmosomes were predominately mechanically removed without undergoing any form of dissolution. Rather, they appear to be torn away from one cell and internalised by its neighbour.

Internalised desmosomes include all major desmosome proteins plus keratin filament fragments

To determine which of the multiple components remained associated with internalised desmosomes after cell separation, we examined their composition using fluorescence super-resolution microscopy following immunostaining for major desmosomal proteins. Structured illumination microscopy (SIM) and co-localisation analysis revealed that the majority of internalised desmosomes maintained their protein composition following internalisation (Fig. 5 A, B). The high resolution of SIM clearly revealed the two distinct patches of DP in the intact desmosomes (Fig. 5 A, lower left panel). This morphology, referred to as “railroad tracks” (Stahley et al., 2016), was also observed post internalisation (Fig. 5 A). Analysis based on images taken by wide field microscopy showed internalised Dsc2a-YFP co-localised with DP (81% of all internalisation events), PG (91%), Pkp1 (72%) and keratin 8 (KRT8, 88%) (Fig. 5 B). These results support the interpretation that the internalised desmosomes were intact, both at the morphological level and in terms of protein composition.

Electron micrographs showed intermediate filaments attached on both sides (plaques) of the internalised desmosomes (Fig. 4 G). Also SIM analysis suggested that internalised desmosomes were still attached to keratin filaments after internalisation (Fig. 5 A, lower right panel). Some of the high-resolution images suggested that keratin filaments were severed at one side of the desmosome originating from the neighbouring cell (Fig. 5 C). To examine this possibility further, we carried out live-cell imaging on cells stably expressing Dsc2a-YFP which were transiently co-transfected with mCherry-KRT18. This resulted in all cells possessing YFP-labelled desmosomes but only a subset showing mCherry-labelled keratin filaments. Where pairs of mCherry-KRT18-expressing cells with K18-untransfected cells were tracked through HGF-induced scattering, co-internalisation of mCherry-KRT18 with Dsc2a-YFP into the non-transfected cell was observed (Fig. 5 D, Movie 2). These results are consistent with the view that the force involved in cell separation results in rupture or severing of the keratin filaments in one of the opposing cells, rather than pulling the desmosome plaques apart from each other. This reinforces the picture of desmosomes as extremely stable cell-cell attachments.

Whole desmosome internalisation is dependent on actin

The internalisation of half desmosomes following chelation of extracellular Ca^{2+} has been shown to be dependent on actin (McHarg et al., 2014). To investigate the role of the actomyosin network in the internalisation of whole desmosomes in our model, MDCK cells were pre-treated for 1 hour with the p160ROCK inhibitor Y-27632 (50 µM), followed by co-treatment with HGF and the inhibitor. Y-27632 attenuated the spreading of the cells and the internalisation of desmosomes (Fig. 6 A, B, Fig. S2 B). Furthermore, staining for actin and a myosin regulatory light chain (MYL12B) as an indicator for active

non-muscle myosin-2 revealed a high co-localisation of stress fibres with DP at last points of contact before desmosomes were internalised when treated with HGF alone (Fig. 6 A, C) (Heissler and Manstein, 2013). Treatments with myosin II inhibitor blebbistatin (50 µM) also debilitated the ability of cells to scatter and the internalisation of desmosomes (Fig. 6 B, Fig. S2 B). These results suggest that actomyosin and thus force is required for internalisation of whole desmosomes during cell scattering.

Desmosome protein mobilities remain consistent after internalisation

Since desmosomes remained structurally intact following internalisation, we next asked whether internalisation changed the stability or the dynamic behaviour of the individual desmosomal components. We therefore analysed FLAP on Dsc2a as part of the stable desmosomal moiety and the putative signalling component Pkp2a in internalised desmosomes after 4h of HGF treatment. Both Dsc2a and Pkp2a showed a comparable FLAP profile following HGF treatment to the PBS control (Fig. 7 A-C). The results indicate that the functional structure of desmosomes, encompassing both the stable moiety and the transiently interacting Pkp2a, remained consistent after internalisation. It remains to be determined whether these internalised structures therefore perform any further function within the cells.

Discussion

Our major finding is that desmosomes consist of two contrasting protein moieties or modules. These are: (1) a strikingly stable module composed of the DCs and PG, at the calcium-dependent stage, and (2) a high mobility module, represented by Pkp2a, which exhibits a transient interaction with the desmosome core and a fast turnover between its desmosome-associated pool and a cytoplasmic pool. Additionally, under these conditions DP in CaCo-2 cells can already be counted as part of the stable moiety. Both modules become less dynamic as desmosomes mature from calcium-dependence to hyper-adhesion. While DP transits to behave more like a stable component at this stage in MDCK cells, Pkp2a in both MDCK and CaCo-2 cells retains high molecular mobility. This modular composition of desmosomes is maintained even during growth factor-induced epithelial cell separation when whole double-plaque-bearing desmosomes are internalised by the scattering MDCK cells (Fig. 8). We further demonstrate that these internalised desmosomes are fully intact and even retain attached, apparently torn keratin filaments from the formerly adjacent cell. This suggests that force is involved during the loss of cell-cell adhesion and cell separation. Inhibition of actomyosin attenuated both cell scattering and the internalisation of desmosomes. It appears that the cells are literally torn apart by the force generated by their scattering movement.

FRAP and FLAP allow detailed analysis of the integration of proteins in subcellular compartments (Ishikawa-Ankerhold et al., 2012). Our study has revealed a diverse profile of protein dynamics of components within desmosomes that are engaged in cell-cell adhesion, the most striking observation being that Pkp2a is highly dynamic throughout desmosome maturation and downregulation, while the

DC adhesion receptors are exceptionally stable. This finding is even more surprising because ultrastructural studies have shown that Pkp is located in the outermost region of the outer dense desmosomal plaque (Al-Amoudi et al., 2007; North et al., 1999). Our results suggest that molecular exchange can take place readily within this apparently dense and well-organised structure. For integrin mediated cell-matrix adhesions (focal adhesions), it was previously shown that structural proteins that directly link adhesion receptors to the contractile actin cytoskeleton are less mobile than proteins controlling fast signalling processes (e.g. GTPase activity) (Stutchbury et al., 2017). By analogy, the interpretation of our data in this study may lead to a model whereby the DCs, PG and DP form the main stable axis to the intermediate filament (IF) network and that Pkps can act as the major signalling components distributing information derived from desmosomes to other compartments of the cell. Such model would be in line with the multiple ways Pkps are involved in a variety of signalling events (Hatzfeld, 2007; Hatzfeld et al., 2014). Two examples that may particularly benefit from fast translocation of Pkp2 to different compartments are its reported roles in regulating RhoA localisation thus mediating signals that also affect the actin cytoskeleton, and in transcriptional regulation in the nucleus (Cerrone et al., 2017; Godsel et al., 2010; Mertens et al., 1996; Sobolik-Delmaire et al., 2010). There is increasing evidence that this occurs in collaboration with components of adherens junctions and the fast cycling Pkp2, potentially through competitive binding with E-cadherin for β-catenin (Chen et al., 2002).

In order to compare proteins dynamics, we have focused on one representative candidate of each desmosomal protein family. However, tissue-specific isoforms of DCs (Dsg1-4, Dsc1-3) and Pkp (Pkp1-3) have been identified and their dynamic properties within desmosomes may differ. In line with our findings, another DC, Dsg3, has been shown to be exceptionally stable in mouse keratinocytes (Vielmuth et al., 2018). The high mobile fraction of Pkp2 in our study also seems to apply to Pkp3, which is present in most simple and stratified epithelia and was shown to have a mobile fraction of approximately 60% in mouse keratinocytes (Keil et al., 2016; Schmidt and Jager, 2005). Pkp1 is more closely related to Pkp2, likewise exhibiting a dual localisation within the karyoplasm and desmosomes though with an expression pattern mostly restricted to complex and suprabasal layers of stratified epithelia thus reciprocally to that of Pkp2 (Schmidt and Jager, 2005). The mobility of Pkp1 has been shown to be dependent on phosphorylation through AKT2 and appears to differ in a cell-type dependent manner with a high mobile fraction of 60% in MCF-7 cells and being considerably more stable (F_m of around 30%) in mouse keratinocytes (Keil et al., 2016; Wolf et al., 2013). It still remains to be clarified what signalling pathways regulate Pkp dynamics and *vice versa*. Nevertheless, these previous findings reinforce the dualistic model of desmosome dynamics where Pkps are part of a desmosomal signalling module.

The mobility of all tested proteins significantly decreased during the maturation from a calcium-dependent to the calcium-independent switch to the hyper-adhesion state in MDCK cells. The already low mobile fractions almost halved for the DCs, PG and DP, and decreased by 15% for Pkp2a. A similar result was found recently when hyper-adhesion was pharmacologically induced with Gö6976, an inhibitor of conventional PKC isoforms, though Pkp was not included in that study (Bartle et al.,

2020). The disadvantage of using such an inhibitor is that it may block multiple cellular events, any one of which may directly or indirectly affect the mobility of desmosomal components. Now that we have studied simple time-dependent maturation of desmosomes, we may be fully confident that stabilisation of desmosomal components is indeed a consequence of hyper-adhesion.

Of particular interest is the decrease in mobility of DP that accompanies desmosome maturation in MDCK cells. During the calcium-dependent phase we found DP to be substantially more mobile than the stable moiety represented by the DCs and PG, but with the onset of hyper-adhesion its mobility was reduced to the extent that it could now also be considered part of the stable moiety. We suggest that this stabilisation of DP makes a significant contribution to the gaining of hyper-adhesion. This view is consistent with data showing that a phospho-null DP mutant with enhanced keratin binding properties leads to an increased association of the desmosomal plaque with keratin filaments, resulting in decreased protein exchange and increased desmosome stability (Albrecht et al., 2015; Bartle et al., 2020). It was proposed that inhibition of PKC inhibitors or downregulation of PKCα may promote DP-keratin integration leading to the onset of hyper-adhesion (Bartle et al., 2020). Furthermore, during formation of the desmosome-keratin scaffold the development of radial and inter-desmosomal keratin filaments coincided with a decrease in DP mobility (Moch et al., 2019). Considering that the mobility of DP was lower in CaCo-2 cells than in MDCK cells, resembling the mobility reported by Bartle et al. in HaCaT cells (Bartle et al., 2020), it would be interesting to speculate that the dynamics of DP are cell-type specific and just one factor driving the onset of hyper-adhesion.

There is also evidence for alternative ways of influencing the mobility of desmosomal proteins, one deriving from crosstalk with the actin cytoskeleton. For example, the knockout of α-adducin, a protein involved in the assembly of a plasma membrane-stabilising cortical spectrin-actin network, increased Dsg3 mobility in the membrane (Hiermaier et al., 2021). Adducin is a PKC substrate (Larsson, 2006), as are many of the actin regulatory proteins. Also, actin-mediated endocytosis is regulated by PKCα and it can be blocked by the inhibitor Gö6976 (Hryciw et al., 2005), as can the actin-mediated internalisation of half-desmosomes (Holm et al., 1993). Furthermore, it has been shown that complete absence of PKCα in mice appears to stabilise hyper-adhesion of desmosomes in epidermal wounds (Thomason et al., 2012). It is thus highly probable that PKCα regulates the mobility and the life cycle of the desmosomal complex at multiple levels, even though it is not required for desmosome assembly (Thomason et al., 2012). Further experiments are needed to determine the precise role of PKCα in the life cycle of desmosomes.

Another possible reason for such decrease in mobility of desmosomal components could be the progressive packing of cadherins into a higher order array that locks DCs in a calcium-independent adhesion state; this increasing order undoubtedly occurs during the onset of hyper-adhesion (Garrod et al., 2005; Kimura et al., 2012). This suggestion was disputed by Bartels and colleagues who found that the ordered packing of Dsg3 with a genetically modified extracellular domain was lost on

chelation of Ca^{2+} from pharmacologically induced hyper-adhesive desmosomes (Bartle et al., 2020). However, the modified Dsg3 may not reflect the behaviour of wild type DCs, since it is difficult to understand how adhesion between opposed desmosomal halves can be maintained in the presence of chelating agents, the defining criterion of hyper-adhesion, if the ordered array of their EC domains is lost (Garrod, 2013).

Irrespective of their maturation state, desmosomes form extremely strong intercellular bonds. Our data demonstrate that cells appear to move apart by tearing part of the desmosome-IF complex out from the neighbouring cell, resulting in the internalisation of the desmosomes as a whole unit with associated keratin filaments. This observation was surprising as others claimed that cell scattering involved desmosome dissociation or junctional splitting together with partial desmosome disassembly (Boyer et al., 1989; Savagner et al., 1997). We found no evidence for such mechanisms of desmosome dismantling in cells undergoing scattering. The forceful internalisation of the whole complex by one of the attached cells recalls the observation of whole desmosome internalisation seen *in vivo* in wound edge keratinocytes and certain carcinomas (Allen and Potten, 1975; Garrod et al., 2005; Schenk, 1975). It is striking that once internalised, desmosomes remained intact as judged by both their ultrastructure and protein composition. The few observed internalised half-desmosomes resembled those described by Demlehner et al. and Duden and Franke in cells in low calcium medium or uncoupled cells and might represent the internalisation of newly assembled half-desmosomes from the membrane (Demlehner et al., 1995; Duden and Franke, 1988). Alternatively, they could represent a small fraction of desmosomes that split in half prior internalisation (Fig. S2 G Model 2). However, the co-localisation experiments and EM analysis revealed that the internalisation of entire desmosomes is by far the dominant mode (> 90%) of desmosome internalisation (Fig. 8, S2 G Model 1). Over longer periods after internalisation we previously showed that components of engulfed desmosomes remained associated and were not recycled, but rather underwent lysosomal and proteasomal degradation (McHarg et al., 2014).

We note that a similar mode of internalisation to that we describe here, that is the internalisation of junctions by one member of a pair of cells, has also been reported for tight junctions and gap junctions (Jordan et al., 2001; Matsuda et al., 2004). However, unlike the internalisation of the whole junctional complex, Matsuda et al. revealed that for tight junctions only the transmembrane proteins, claudin-3 and -1, of apposed membranes were co-endocytosed (Matsuda et al., 2004). Whereas other tight junction components seemed to have dissociated from those claudins prior to their internalisation. Jordan et al. described a similar co-endocytosis of connexin-based gap junctions but noted that those internalised gap junctions, referred to as annular junctions, are rare and unlikely the only mechanism to clear gap junctions from the plasma membrane (Jordan et al., 2001).

In their study of scattering by NBT II cells, Boyer et al. noted that loss of cell-cell contact was accompanied by the appearance within the cytoplasm of dots containing desmosomal components and associated keratin filaments (Boyer et al., 1989). We suggest that these dots were equivalent to the whole internalised desmosomes that we report here. We have further shown that some of these filaments are contributed by the opposing cell of an adjacent pair, indicating that the filaments have been fragmented during cell separation. If we take the view that cell separation occurs by tearing under the force generated by cell movement, this would suggest that the keratin filaments have simply broken under the applied force. Our data show that stress fibres accumulate at sites of desmosomes after HGF treatment and the presence of actomyosin indicate that these sites are under tension. This enrichment of actomyosin at desmosomes disappeared in presence of actomyosin inhibitors and the cells failed to separate. These experiments suggest that forces are critical for cell separation at the sites of desmosomes. Alternatively, we may speculate that a signalling event such as phosphorylation is involved in severing the keratin filaments and that such a signalling process would therefore have a facilitating role in cell separation. This would be analogous to the rapid and specific phosphorylation events that sever cytoskeleton components for daughter cell separation at the end of cytokinesis and during meiotic maturation (Goto et al., 2000; Klymkowsky et al., 1991). Our data do not address the severing mechanism in particular, but, given the particular high tensile strength of keratins (Qin et al., 2010), it seems likely that the breakage involves additional processes.

In conclusion, our data represented here leads to a new concept of dualistic desmosome organisation. There appear to be two protein moieties or modules within the junctions, i.e. a stable moiety which is presumably responsible for the strong adhesive function of the desmosome, and a much more mobile protein moiety, exemplified by Pkp2a, which has the potential for signalling and regulatory function. This behavioural dichotomy is both present and detectable when desmosomes are relatively newly formed and calcium-dependent, and when they mature to calcium-independence. This dualism persists even when desmosomes are being down-regulated and removed.

Materials and Methods

Cell lines and transfection

Madin-Darby canine kidney II cells (MDCK) (Madin and Darby, 1958) (ECACC) and the human colon adenocarcinoma cell line CaCo-2 (CaCo-2) (Fogh et al., 1977) (ATCC, kindly provided by I.Roberts, University of Manchester, Manchester) were cultured at 37°C in 5% humidified CO_2 in high glucose Dulbecco's Modified Eagle Medium (DMEM, Sigma or GE Healthcare), supplemented with 10% (v/v) foetal calf serum (FCS, Gibco or GE Healthcare) and 100 U/ml penicillin and 100 μg/ml streptomycin (P/S; Gibco), herein referred to as standard medium (SM) with a calcium concentration of approximately 1.8 mM. Cells were transfected using Lipofectamine LTX transfection reagent, according to the manufacturer's instructions (Invitrogen). To generate stable cell lines transfected MDCK cells were selected using 2μg/ml puromycin (Thermofisher) in SM with medium changes every two days for 10 days. MDCK cells stably expressing Dsc2a-YFP were kindly provided by R.E.Leube,

University Hospital RWTH, Aachen (Windoffer et al., 2002). CaCo-2 cells were transiently transfected using Lipofectamine LTX, plated on glass-bottom dishes (MaTek) and imaged 24 h post transfection. For live-cell imaging experiments, MDCK cells were plated on glass-bottom dishes (MatTek or Ibidi). For cell scattering experiments using HGF, the glass-bottom dishes were coated with 10 μg/ml bovine plasma fibronectin (FN; Sigma) diluted in PBS.

Cloning and constructs

DP-eGFP (#32227), Dsg2-mCherry (#36991) and mCherry-KRT18 (#55065) were purchased from Addgene. mEmerald-E-cadherin was obtained from the Michael Davidson collection #54072 from P. Kanchanawong (Mechanobiology Institute, Singapore). Dsc2a-YFP was a kind gift from R. E. Leube (University Hospital RWTH, Aachen). To generate constructs containing PaGFP, neonGreen and mScarlet, we have used plasmids where the desmosome genes were already cloned into a custom-made vector by Oxford Genetics where the vector pSF (#OG394R1) was modified to have an EF1a promoter and puromycin selection marker. The vector was linearized by restriction digestion followed by gel purification (see Table S2 for restriction enzymes used), and the purified vector was used to clone fragments containing the ORFs of PaGFP, neonGreen and mScarlet, these fragments were amplified by Polymerase Chain Reaction using Phusion® High-Fidelity DNA Polymerase (M0530L, New England Biolabs (NEB)) using 35 cycles with an annealing temperature of 60 °C (see Table S2 for list of primers) and cloned by Gibson Assembly Cloning Kit (#EE5510S, NEB). All primers were designed using SnapGene (GSL Biotech LLC, Chicago, IL) and were synthesised by Eurofins Genomics (Germany). All ORF sequences were confirmed by Sanger sequencing by Eurofins.

Antibodies and reagents

The following antibodies were used at the indicated dilutions (in 1% BSA in PBS (Sigma)): anti-desmoplakin I and II (clone 11-5F, D. R. Garrod), 1:400; anti-plakoglobin (clone 15F11, Sigma), 1:100; 1:100; anti-keratin 8 (clone LE41, E. B. Lane), used as hybridoma culture supernatant; anti-Dsc2/3 (clone 7G6, Zymed Laboratories), 1:100; anti-plakophilin 1 (clone PP1-5C2, Abnova), 1:50; anti-MYL12B (also known as MRLC2, clone EPR9331, Abcam), 1:100. Secondary antibodies conjugated to Alexa Fluor 488, 594 or 647 were all from Thermofisher (used at 1:500). Alexa Fluor 488- (1:500), Texas-Red-X- (1:500) and Alexa Fluor 647-conjugated (1:200) phalloidin were from Life Technologies. DAPI readymade solution (Sigma) was used at a concentration of 1μg/ml. Y-27632 dihydrochloride (Tocris Bioscience) was dissolved in water and used at a final concentration of 50 μM. blebbistatin (Tocris Bioscience) was diluted in DMSO (Sigma) and used at a final concentration of 50 μM.

Calcium switch assay

MDCK cells were cultured at confluent density (1.35 x 10^5 cells/cm^2) in SM for 1 d or 3 d. They were washed thrice with calcium- and magnesium-free PBS (Gibco) and incubated with calcium-free DMEM (Gibco) supplemented with 10% chelated FBS and 3 mM EGTA (Sigma-Aldrich), herein referred to as "+EGTA" for 90 min (unless specified otherwise) at 37°C 5% humidified CO_2. Calcium

sensitivity of desmosomes was quantified as previously described (Wallis et al., 2000). In brief, following Ca^{2+}-chelation, the cells were fixed in ice-cold methanol for 10 min and immunostained for desmoplakin by immunofluorescence. Cells which remained attached by desmoplakin positive projections were scored as having calcium-independent desmosomes and expressed proportional to the total cell number.

Cell scattering assay

Transfected MDCK cells were plated at $1.5x10^3$ cells/cm^2 on FN coated glass-bottom dishes and cultured in SM for 2 d at 37°C. The cells were serum starved for 12 h in DMEM supplemented with 1% P/S (serum free medium, SFM). Cells were treated with 40 ng/ml human recombinant hepatocyte growth factor (HGF; STEMCELL Technologies) in SFM for 4 h at 37°C prior to live-cell imaging or 6 h prior to fixation and staining. Scattering was assessed by immunostaining for desmoplakin and quantified by scoring cells, which remained attached with desmosomes to only two neighbouring cells. These scattering cells were expressed proportional to the total number of cells in the cell islets.

Drug treatment

MDCK wild-type (wt) cells were cultured in the same manner as for the cell scattering assay, but prior to treatment with HGF the cells were pre-treated for 1 h with SFM supplemented with either Y-27632 (50 µM) or blebbistatin (50 µM). HGF at a final concentration of 40 ng/ml was added to the drug treatment and cells were cultured for 6 h prior fixation and immunostaining for DP, actin and MYL12B.

Microscopy

Co-localisation experiments were carried out using a Delta Vision microscope (Applied Precision) 60x/1.42 Plan Apo N (Oil) objective and a Sedat Quad filter set, with images collected using a Retiga R6 (Q-Imaging) camera.

3D-SIM was performed using a DeltaVision OMX Version 4 Blaze microscope (GE Healthcare), equipped with 405-, 488-, and 568-nm lasers and a BGR filter drawer. A 100x/1.40 PSF Plan Apo Oil objective and liquid-cooled Photometrics Evolve EM charge-coupled device camera for each channel were used. For 3D-SIM, 15 images per section per channel were acquired (made up of 3 rotations and 5 phase movements of the diffraction grating) at a z-spacing of 0.125 µm. Structured illumination reconstruction and alignment were carried out using the SoftWoRx (GE Healthcare) program.

FLAP, FRAP and HGF-induced scattering experimental data of MDCK cells was collected with an inverted Nikon Eclipse Ti microscope equipped with a 100×/NA 1.40 Plan Apo oil immersion objective lens, a focus drift correction system, a piezo-motorized stage, a 37 °C on-stage incubation system (LCI), 100 mW diode lasers (405 nm, 491 nm and 561 nm), an EMCCD camera (Evolve 512; Photometrics), CSU-22 spinning disk scan head (Yokogawa) and a 3D FRAP system (iLAS2 Roper Scientific). The microscope system was controlled using MetaMorph (Molecular Devices) and iLAS2 (Roper Scientific) software.

FLAP and FRAP experimental data of CaCo-2 cells was acquired using a CSU-X1 spinning disc confocal (Yokagowa) on a Zeiss Axio-Observer Z1 microscope with a 60x/1.40 Plan-Apochromat objective, Evolve EMCCD camera (Photometrics) and motorised XYZ stage (ASI). The 488nm, 561nm and 405nm lasers were controlled using an AOTF through the laserstack (Intelligent Imaging Innovations (3I)) allowing both rapid 'shuttering' of the laser and attenuation of the laser power. The microscope system was controlled using Slidebook software (3I).

Immunofluorescence microscopy

Cells were fixed with 4% (w/v) paraformaldehyde in PBS or 100% ice-cold Methanol for anti-desmoplakin (clone 11-5F) immunostaining. Antibodies were diluted in 1% BSA and added to the cells for 1h. Images were acquired on the Delta Vision systems (above) and processed using the FIJI-ImageJ software (version 1.53g). To analyse co-localisation, background was subtracted using a rolling ball algorithm, thresholding was performed using ImageJ's triangle algorithm based on the Dsc2a-YFP intensity and the particle analysis function of ImageJ was used to identify Dsc2a-YFP particles in a region of interest. These particles were manually assessed for co-localisation with the protein of interest using ImageJ's RGB profiler's function. Results were calculated as percentages of co-localising events. To quantify cytoplasmic desmosomes, cells were first immunostained for DP. Images were thresholded using ImageJ's triangle algorithm and particles of a minimum size of 20 nm^2 were measured within the cytoplasm 2 µm away from the membrane.

Live-cell imaging

FRAP

MDCK cells stably expressing neonGreen, mEmerald or eGFP constructs were seeded at confluent density (1.35 x 10^5 cells/cm^2) on uncoated glass bottom dishes in SM and cultured for 24 hours for Ca^{2+}-dependent desmosomes or for 3 days for desmosomes to acquire hyper-adhesion before imaging. CaCo-2 cells were imaged 24 hours following transfection. Images of MDCK cells were acquired using the Nikon Eclipse Ti system (see above) and those of CaCo-2 cells using the Zeiss Axio-Observer Z1 system (see above). For FRAP quantification five ROIs of 2 µm diameter circles at the cell-cell junctions were selected and photobleached with a 10 ms burst of the 488 nm laser at 100% power. iLAS2 or Slidebook software was used to capture three images prior to photobleaching and one image every 10 s for 5 min to 10 min post bleaching. Movies were analysed using Fiji (version 1.53g) by manually tracking the ROI and measuring the fluorescence signal. The subsequent analysis was performed as described previously (Carisey et al., 2011). In brief, intensities of bleached ROIs and three control unbleached desmosomal ROIs were manually measured using ImageJ. Values were background subtracted and measurements were corrected with the control values of unbleached ROIs to compensate for any overall loss of fluorescence. The values were then normalised to the intensity of the first postbleach value. Graphs were prepared using Prism 8 (GraphPad).

FLAP

MDCK cells co-expressing the required PaGFP-tagged constructs and a mScarlet-tagged desmosome marker protein (Dsc2a-mScarlet unless otherwise specified) were plated at confluent density (1.35 x 10^5 cells/cm^2) on uncoated glass bottom dishes and cultured for 24 h or 3 d before imaging. To measure protein dynamics following cell scattering imaging started 4 h post HGF treatment, local sites of cell separation were observed and ROIs of internalised desmosomes were selected. CaCo-2 cells were imaged 24 hours following transfection. Images of MDCK cells were acquired using the Nikon Eclipse Ti system (see above) and those of CaCo-2 cells using the Zeiss Axio-Observer Z1 system (see above). Similarly to FRAP five ROIs of 2 µm diameter circles were selected and photoactivated using a 405 nm laser at 100% power for 10 ms. iLAS2 or Slidebook software was used to capture three images prior and one image every 10 s for 5 min up to 1 h post photoactivation. Movies were analysed using Fiji (version 1.53g). The intensities of the postactivated PaGFP ROIs were measured manually using ImageJ. Values were normalized to the intensity of the first postactivation image. Graphs were prepared using Prism 8 (GraphPad).

CLEM

MDCK cells stably expressing Dsc2a-YFP were co-cultured with MDCK cells transiently expressing Dsg2-mCherry on a gridded glass-bottom dish (MatTek). Cells were treated with HGF (see above). Live-cell imaging of regions of interest (ROI) was carried out using the Nikon Ti Eclipse microscope (see above). Cells were grown on glass-bottom dish with gridded coverslip (MatTek Corporation, Part No: P35G-1.5-14-CGRD). After fluorescence images of cells co-expressing Dsc2a-YFP and Dsg2-mCherry were acquired, bright field (phase contrast) images of cells and finder grid index were captured at lower magnification for ROI reference. Cells in dishes were then fixed with 2% glutaraldehyde and 4% formaldehyde in 0.1M Cacodylate buffer, post-fixed in 1% Osmium tetroxide, dehydrated in ethanol and embedded in Epoxy resin (EPON 812, SERVA). Upon resin polymerization the coverslip was removed using liquid nitrogen (leaving finder-grid embossed to the block surface) and respective ROI were re-localized under stereomicroscope. Target cells within ROI were cut horizontally with ultramicrotome (LEICA Ultracut-UC7), ultrathin sections collected on formvar/carbon-coated slot grids (Ted Pella Inc., #01805-F) and post-contrasted with Uranyl Acetate and Lead Citrate. Sections were analysed under JEOL JEM-1010 transmission electron microscope operated at 80kV and images acquired with SIA 12C CCD camera. Desmosome width was measured by taking the average of three line measurements per desmosome using ImageJ. 10 desmosomes each of 10 cells (N=3) at the membrane and following internalisation were measured.

Statistical analysis

Graphing and statistical analysis were performed by using GraphPad Prism 8 and 9 software. When comparing means, the D'Agostino–Pearson test was used to assess the normality of the data to determine the appropriate statistical tests to use.

Acknowledgements

This work was supported by the Faculty of Biology, Medicine and Health at the University of Manchester, UK and by the Agency for Science, Technology and Research (A*STAR), Singapore. We thank the staff of the Bioimaging facility at the University of Manchester and the A*STAR Microscopy Platform for their help with imaging and analysis. C. Ballestrem acknowledges the Biotechnology and Biological Sciences Research Council (BBSRC, grant numbers BB/R001707/1, BB/R014361/1) and the Wellcome Trust (grant number 202923/Z/16/Z) for funding of this project. The C. Ballestrem laboratory is part of the Wellcome Trust Centre for Cell-Matrix Research, University of Manchester, which is supported by core funding from the Wellcome Trust (grant number 203128/Z/16/Z). The work in Singapore was supported by institutional core funding to the Skin Research Institute of Singapore from the Biomedical Research Council of Singapore. J. Fülle is supported by the Faculty of Biology, Medicine and Health at the University of Manchester and by the Agency of Science Technology and Research (A*STAR).

The authors declare no competing financial interests.

Author contributions: JBF, HH, DG and CB designed experiments, with input from EBL and GDW. JBF, HH, DL and JL performed the experiments and analysed the data. RA and BY provided assistance with generation of tagged desmosomal constructs. Figures were prepared by JBF. JBF, DG, EBL and CB wrote the manuscript. CB, DG, GDW and EBL supervised the project and acquired funding.

References

Al-Amoudi, A., D.C. Díez, M.J. Betts, and A.S. Frangakis. 2007. The molecular architecture of cadherins in native epidermal desmosomes. *Nature*. 450:832–837.

Albrecht, L.V., L. Zhang, J. Shabanowitz, E. Purevjav, J.A. Towbin, D.F. Hunt, and K.J. Green. 2015. GSK3- and PRMT-1-dependent modifications of desmoplakin control desmoplakin-cytoskeleton dynamics. *J Cell Biol*. 208:597-612.

Allen, T.D., and C.S. Potten. 1975. Desmosomal form, fate, and function in mammalian epidermis. *J Ultrastruct Res*. 51:94-105.

Balkovetz, D.F. 1998. Hepatocyte growth factor and Madin-Darby canine kidney cells: in vitro models of epithelial cell movement and morphogenesis. *Microsc Res Tech*. 43:456-463.

Bartle, E.I., T.C. Rao, R.R. Beggs, W.F. Dean, T.M. Urner, A.P. Kowalczyk, and A.L. Mattheyses. 2020. Protein exchange is reduced in calcium-independent epithelial junctions. *J Cell Biol*. 219.

Bartle, E.I., T.M. Urner, S.S. Raju, and A.L. Mattheyses. 2017. Desmoglein 3 Order and Dynamics in Desmosomes Determined by Fluorescence Polarization Microscopy. *Biophys J*. 113:2519-2529.

Becker, W. 2012. Fluorescence lifetime imaging - techniques and applications. *J Microsc*. 247:119-136.

Boyer, B., G.C. Tucker, A.M. Valles, J. Gavrilovic, and J.P. Thiery. 1989. Reversible transition towards a fibroblastic phenotype in a rat carcinoma cell line. *Int J Cancer Suppl*. 4:69-75.

Carisey, A., M. Stroud, R. Tsang, and C. Ballestrem. 2011. Fluorescence recovery after photobleaching. *Methods Mol Biol*. 769:387-402.

Cerrone, M., J. Montnach, X. Lin, Y.T. Zhao, M. Zhang, E. Agullo-Pascual, A. Leo-Macias, F.J. Alvarado, I. Dolgalev, T.V. Karathanos, K. Malkani, C.J.M. Van Opbergen, J.J.A. van Bavel, H.Q. Yang, C. Vasquez, D. Tester, S. Fowler, F. Liang, E. Rothenberg, A. Heguy, G.E. Morley, W.A. Coetzee, N.A. Trayanova, M.J. Ackerman, T.A.B. van Veen, H.H. Valdivia, and M. Delmar. 2017. Plakophilin-2 is required for transcription of genes that control calcium cycling and cardiac rhythm. *Nat Commun*. 8:106.

Chen, X., S. Bonne, M. Hatzfeld, F. van Roy, and K.J. Green. 2002. Protein binding and functional characterization of plakophilin 2. Evidence for its diverse roles in desmosomes and beta -catenin signaling. *J Biol Chem*. 277:10512-10522.

Chidgey, M., and C. Dawson. 2007. Desmosomes: a role in cancer? *Br J Cancer*. 96:1783-1787.

Delmar, M., and W.J. McKenna. 2010. The cardiac desmosome and arrhythmogenic cardiomyopathies: from gene to disease. *Circ Res*. 107:700-714.

Demlehner, M.P., S. Schäfer, C. Grund, and W.W. Franke. 1995. Continual assembly of half-desmosomal structures in the absence of cell contacts and their frustrated endocytosis: A coordinated Sisyphus cycle. *The Journal of cell biology*. 131:745–760.

Duden, R., and W.W. Franke. 1988. Organization of desmosomal plaque proteins in cells growing at low calcium concentrations. *J Cell Biol*. 107:1049-1063.

Dukes, J.D., P. Whitley, and A.D. Chalmers. 2011. The MDCK variety pack: choosing the right strain. *BMC Cell Biol*. 12:43.

Dusek, R.L., and L.D. Attardi. 2011. Desmosomes: New perpetrators in tumour suppression. *Nat Rev Cancer*. 11:317–323.

Fogh, J., W.C. Wright, and J.D. Loveless. 1977. Absence of HeLa cell contamination in 169 cell lines derived from human tumors. *J Natl Cancer Inst*. 58:209-214.

Foote, H.P., K.D. Sumigray, and T. Lechler. 2013. FRAP analysis reveals stabilization of adhesion structures in the epidermis compared to cultured keratinocytes. *PLoS One*. 8:e71491.

Garrod, D., and M. Chidgey. 2008. Desmosome structure, composition and function. *Biochimica et biophysica acta*. 1778:572–587.

Garrod, D.R. 2013. The assay that defines desmosome hyper-adhesion. *J Invest Dermatol*. 133:576–577.

Garrod, D.R., M.Y. Berika, W.F. Bardsley, D. Holmes, and L. Tabernero. 2005. Hyper-adhesion in desmosomes: Its regulation in wound healing and possible relationship to cadherin crystal structure. *J Cell Sci*. 118:5743–5754.

Gloushankova, N.A., T. Wakatsuki, R.B. Troyanovsky, E. Elson, and S.M. Troyanovsky. 2003. Continual assembly of desmosomes within stable intercellular contacts of epithelial A-431 cells. *Cell Tissue Res*. 314:399-410.

Godsel, L.M., A.D. Dubash, A.E. Bass-Zubek, E.V. Amargo, J.L. Klessner, R.P. Hobbs, X. Chen, and K.J. Green. 2010. Plakophilin 2 couples actomyosin remodeling to desmosomal plaque assembly via RhoA. *Mol Biol Cell*. 21:2844–2859.

Goto, H., H. Kosako, and M. Inagaki. 2000. Regulation of intermediate filament organization during cytokinesis: possible roles of Rho-associated kinase. *Microsc Res Tech*. 49:173-182.

Green, K.J., A. Jaiganesh, and J.A. Broussard. 2019. Desmosomes: Essential contributors to an integrated intercellular junction network. *F1000Res*. 8.

Hatzfeld, M. 2007. Plakophilins: Multifunctional proteins or just regulators of desmosomal adhesion? *Biochimica et biophysica acta*. 1773:69–77.

Hatzfeld, M., A. Wolf, and R. Keil. 2014. Plakophilins in desmosomal adhesion and signaling. *Cell Commun Adhes*. 21:25-42.

Heissler, S.M., and D.J. Manstein. 2013. Nonmuscle myosin-2: mix and match. *Cell Mol Life Sci*. 70:1-21.

Hiermaier, M., F. Kliewe, C. Schinner, C. Studle, I.P. Maly, M.T. Wanuske, V. Rotzer, N. Endlich, F. Vielmuth, J. Waschke, and V. Spindler. 2021. The Actin-Binding Protein alpha-Adducin Modulates Desmosomal Turnover and Plasticity. *J Invest Dermatol*. 141:1219-1229 e1211.

Holm, P.K., S.H. Hansen, K. Sandvig, and B. van Deurs. 1993. Endocytosis of desmosomal plaques depends on intact actin filaments and leads to a nondegradative compartment. *Eur J Cell Biol*. 62:362-371.

Hryciw, D.H., C.A. Pollock, and P. Poronnik. 2005. PKC-alpha-mediated remodeling of the actin cytoskeleton is involved in constitutive albumin uptake by proximal tubule cells. *Am J Physiol Renal Physiol*. 288:F1227-1235.

Ishida-Yamamoto, A., and S. Igawa. 2014. Genetic skin diseases related to desmosomes and corneodesmosomes. *J Dermatol Sci*. 74:99-105.

Ishikawa-Ankerhold, H.C., R. Ankerhold, and G.P.C. Drummen. 2012. Advanced Fluorescence Microscopy Techniques—FRAP, FLIP, FLAP, FRET and FLIM. *Molecules*. 17:4047–4132.
Jordan, K., R. Chodock, A.R. Hand, and D.W. Laird. 2001. The origin of annular junctions: a mechanism of gap junction internalization. *J Cell Sci*. 114:763-773.
Keil, R., K. Rietscher, and M. Hatzfeld. 2016. Antagonistic Regulation of Intercellular Cohesion by Plakophilins 1 and 3. *J Invest Dermatol*. 136:2022-2029.
Kimura, T.E., A.J. Merritt, and D.R. Garrod. 2007. Calcium-independent desmosomes of keratinocytes are hyper-adhesive. *J Invest Dermatol*. 127:775–781.
Kimura, T.E., A.J. Merritt, F.R. Lock, J.J. Eckert, T.P. Fleming, and D.R. Garrod. 2012. Desmosomal adhesiveness is developmentally regulated in the mouse embryo and modulated during trophectoderm migration. *Developmental biology*. 369:286–297.
Klymkowsky, M.W., L.A. Maynell, and C. Nislow. 1991. Cytokeratin phosphorylation, cytokeratin filament severing and the solubilization of the maternal mRNA Vg1. *J Cell Biol*. 114:787-797.
Larsson, C. 2006. Protein kinase C and the regulation of the actin cytoskeleton. *Cell Signal*. 18:276-284.
Lowndes, M., S. Rakshit, O. Shafraz, N. Borghi, R.M. Harmon, K.J. Green, S. Sivasankar, and W.J. Nelson. 2014. Different roles of cadherins in the assembly and structural integrity of the desmosome complex. *J Cell Sci*. 127:2339-2350.
Madin, S.H., and N.B. Darby, Jr. 1958. Established kidney cell lines of normal adult bovine and ovine origin. *Proc Soc Exp Biol Med*. 98:574-576.
Maruthappu, T., A. Posafalvi, S. Castelletti, P.J. Delaney, P. Syrris, E.A. O'Toole, K.J. Green, P.M. Elliott, P.D. Lambiase, A. Tinker, W.J. McKenna, and D.P. Kelsell. 2019. Loss-of-function desmoplakin I and II mutations underlie dominant arrhythmogenic cardiomyopathy with a hair and skin phenotype. *Br J Dermatol*. 180:1114-1122.
Matsuda, M., A. Kubo, M. Furuse, and S. Tsukita. 2004. A peculiar internalization of claudins, tight junction-specific adhesion molecules, during the intercellular movement of epithelial cells. *J Cell Sci*. 117:1247-1257.
Mattey, D.L., and D.R. Garrod. 1986. Splitting and internalization of the desmosomes of cultured kidney epithelial cells by reduction in calcium concentration. *J Cell Sci*. 85:113-124.
McHarg, S., G. Hopkins, L. Lim, and D. Garrod. 2014. Down-regulation of desmosomes in cultured cells: The roles of PKC, microtubules and lysosomal/proteasomal degradation. *PLoS One*. 9:e108570.
Mertens, C., C. Kuhn, and W.W. Franke. 1996. Plakophilins 2a and 2b: Constitutive proteins of dual location in the karyoplasm and the desmosomal plaque. *The Journal of cell biology*. 135:1009–1025.
Moch, M., N. Schwarz, R. Windoffer, and R.E. Leube. 2019. The keratin-desmosome scaffold: pivotal role of desmosomes for keratin network morphogenesis. *Cell Mol Life Sci*.
Nieto, M.A., R.Y. Huang, R.A. Jackson, and J.P. Thiery. 2016. EMT: 2016. *Cell*. 166:21-45.
North, A.J., W.G. Bardsley, J. Hyam, E.A. Bornslaeger, H.C. Cordingley, B. Trinnaman, M. Hatzfeld, K.J. Green, A.I. Magee, and D.R. Garrod. 1999. Molecular map of the desmosomal plaque. *J Cell Sci*. 112 (Pt 23):4325–4336.
Qin, Z., M.J. Buehler, and L. Kreplak. 2010. A multi-scale approach to understand the mechanobiology of intermediate filaments. *J Biomech*. 43:15-22.
Ridley, A.J., P.M. Comoglio, and A. Hall. 1995. Regulation of scatter factor/hepatocyte growth factor responses by Ras, Rac, and Rho in MDCK cells. *Mol Cell Biol*. 15:1110-1122.
Savagner, P., K.M. Yamada, and J.P. Thiery. 1997. The zinc-finger protein slug causes desmosome dissociation, an initial and necessary step for growth factor-induced epithelial-mesenchymal transition. *J Cell Biol*. 137:1403-1419.
Schenk, P. 1975. Desmosomale strukturen im cytoplasma normaler und pathologischer keratinocyten. *Archives of Dermatological Research*. 253:23-42.
Schmidt, A., and S. Jager. 2005. Plakophilins--hard work in the desmosome, recreation in the nucleus? *Eur J Cell Biol*. 84:189-204.
Sinnecker, D., P. Voigt, N. Hellwig, and M. Schaefer. 2005. Reversible photobleaching of enhanced green fluorescent proteins. *Biochemistry*. 44:7085-7094.
Sobolik-Delmaire, T., R. Reddy, A. Pashaj, B.J. Roberts, and J.K. Wahl, 3rd. 2010. Plakophilin-1 localizes to the nucleus and interacts with single-stranded DNA. *J Invest Dermatol*. 130:2638-2646.

Spindler, V., R. Eming, E. Schmidt, M. Amagai, S. Grando, M.F. Jonkman, A.P. Kowalczyk, E.J. Müller, A.S. Payne, C. Pincelli, A.A. Sinha, E. Sprecher, D. Zillikens, M. Hertl, and J. Waschke. 2018. Mechanisms Causing Loss of Keratinocyte Cohesion in Pemphigus. *J Invest Dermatol*. 138:32–37.

Stahley, S.N., M.F. Warren, R.J. Feldman, R.A. Swerlick, A.L. Mattheyses, and A.P. Kowalczyk. 2016. Super-Resolution Microscopy Reveals Altered Desmosomal Protein Organization in Tissue from Patients with Pemphigus Vulgaris. *J Invest Dermatol*. 136:59-66.

Stutchbury, B., P. Atherton, R. Tsang, D.Y. Wang, and C. Ballestrem. 2017. Distinct focal adhesion protein modules control different aspects of mechanotransduction. *J Cell Sci*. 130:1612-1624.

Thomason, H.A., N.H. Cooper, D.M. Ansell, M. Chiu, A.J. Merrit, M.J. Hardman, and D.R. Garrod. 2012. Direct evidence that PKCα positively regulates wound re-epithelialization: Correlation with changes in desmosomal adhesiveness. *The Journal of pathology*. 227:346–356.

Vielmuth, F., M.T. Wanuske, M.Y. Radeva, M. Hiermaier, D. Kugelmann, E. Walter, F. Buechau, T.M. Magin, J. Waschke, and V. Spindler. 2018. Keratins Regulate the Adhesive Properties of Desmosomal Cadherins through Signaling. *J Invest Dermatol*. 138:121-131.

Wallis, S., S. Lloyd, I. Wise, G. Ireland, T.P. Fleming, and D. Garrod. 2000. The alpha isoform of protein kinase C is involved in signaling the response of desmosomes to wounding in cultured epithelial cells. *Mol Biol Cell*. 11:1077–1092.

Windoffer, R., M. Borchert-Stuhlträger, and R.E. Leube. 2002. Desmosomes: Interconnected calcium-dependent structures of remarkable stability with significant integral membrane protein turnover. *J Cell Sci*. 115:1717–1732.

Wolf, A., K. Rietscher, M. Glass, S. Huttelmaier, M. Schutkowski, C. Ihling, A. Sinz, A. Wingenfeld, A. Mun, and M. Hatzfeld. 2013. Insulin signaling via Akt2 switches plakophilin 1 function from stabilizing cell adhesion to promoting cell proliferation. *J Cell Sci*. 126:1832-1844.

Figures

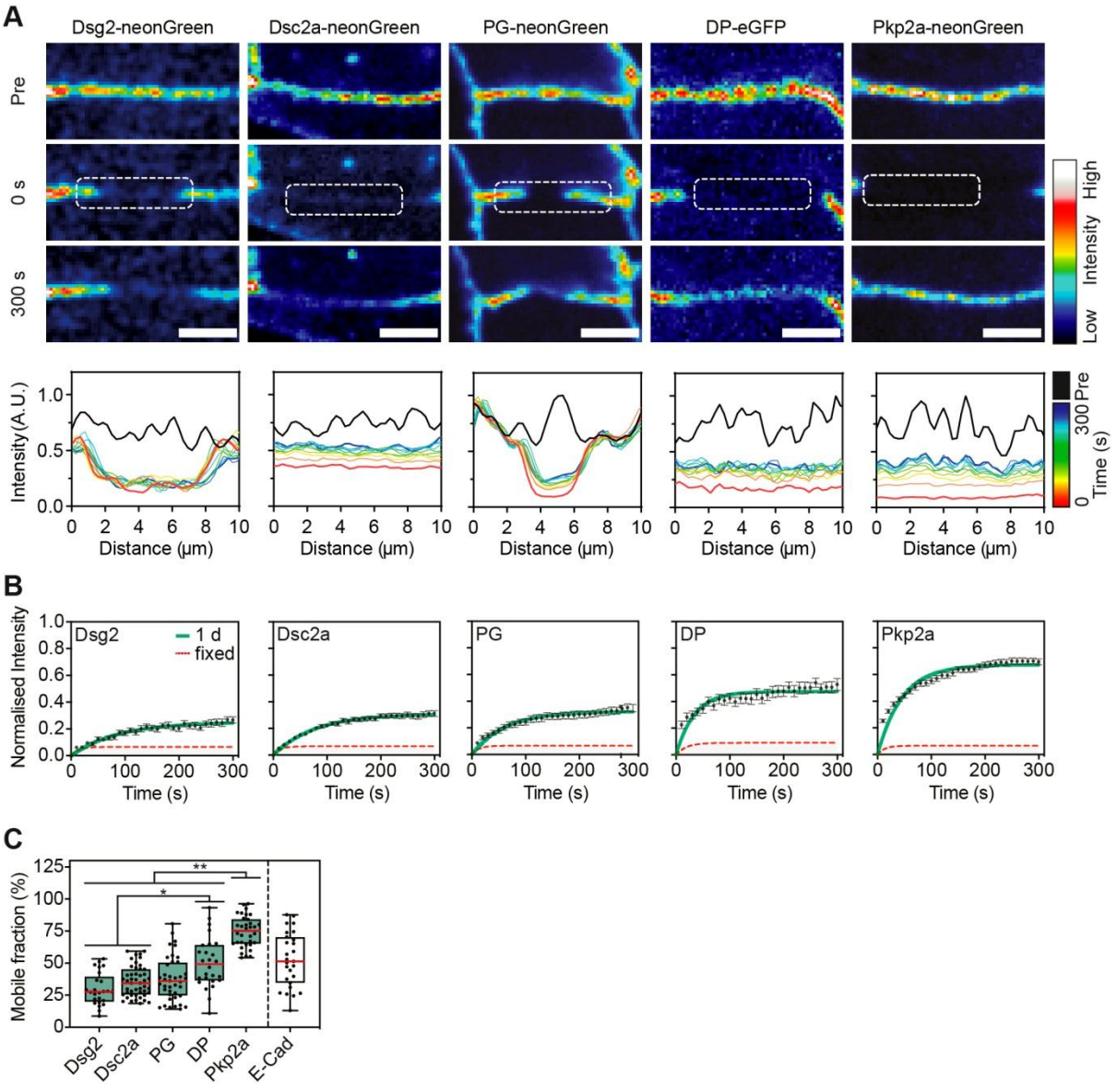

Figure 1. Calcium-dependent desmosomes exhibit differential protein dynamics. (A) Representative time-lapse images showing FRAP in MDCK cells transfected with neonGreen-labelled desmoglein 2 (Dsg2), desmocollin 2a (Dsc2a), plakoglobin (PG) and plakophilin2a (Pkp2a), and eGFP tagged desmoplakin (DP). The cells were cultured confluent for 1 d before recording with the majority of desmosomes being calcium-dependent. Images are presented in a colour intensity scale. Graphs show the line profile plots of the bleached ROIs (dashed box at 0 s) over time in a colour intensity scale. Scale bar: 5 μm. Note the recovery of Pkp2a in similar spots as pre-bleaching. (B) Graphs show the mean fluorescence recovery

curves for all recorded desmosomes (n=24-47, N=3), error bars are ±s.e.m.; red line showing the recovery of PFA-fixed samples (reversible photobleaching). (C) Mean mobile fraction values for the indicated desmosomal proteins in MDCK cells (scatter plot). (n=24-47, N=3). The box represents the 25-75th percentiles, and the median is indicated in red. The whiskers show the range of values. **P ≤ 0.01; *P ≤ 0.05 (Kruskal-Wallis with Dunn's multiple comparisons test).

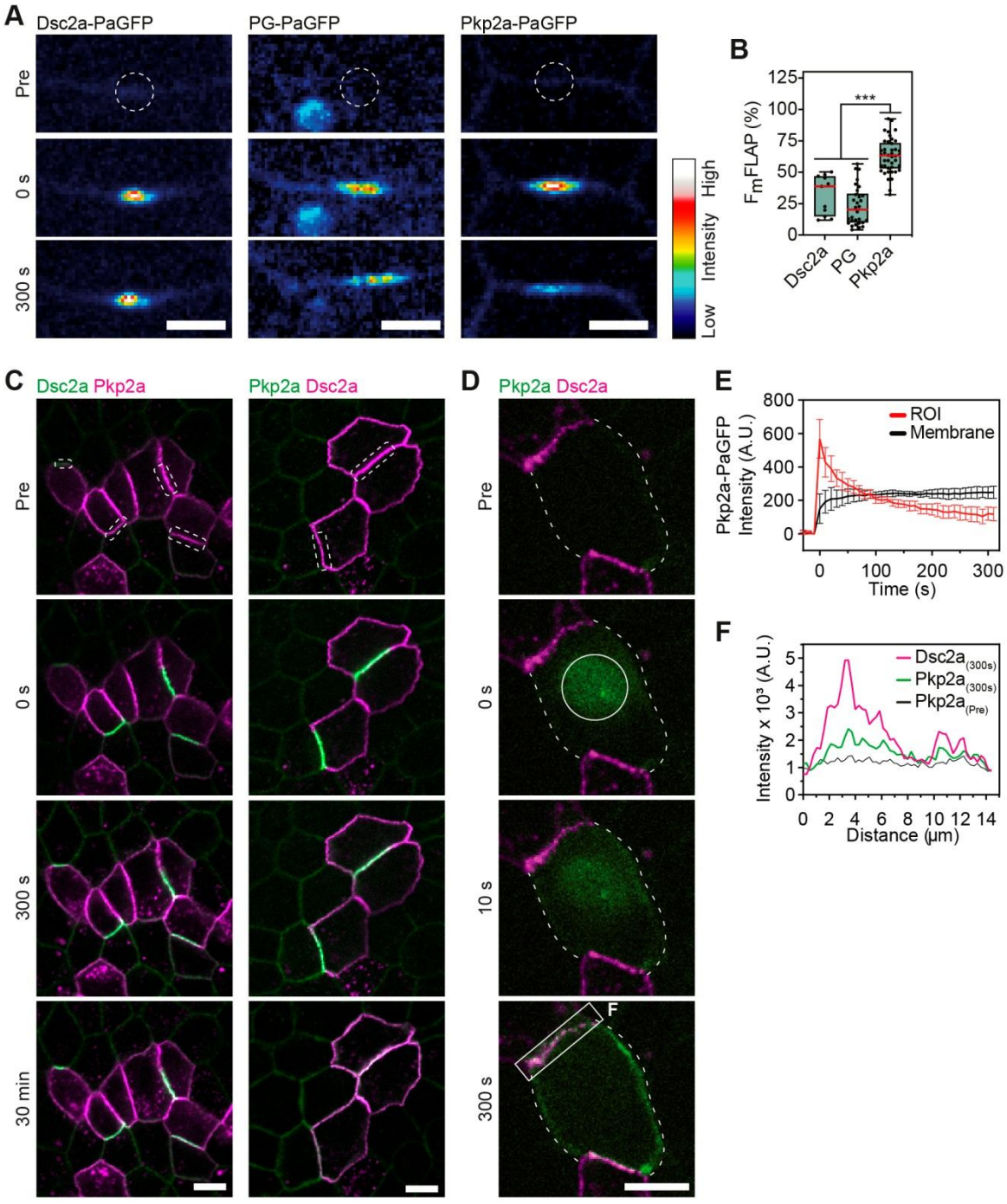

Figure 2. Cytoplasmic pool of plakophilin 2a enables rapid exchange at desmosomes. (A) Representative time-lapse images showing FLAP in MDCK cells stably expressing photoactivatable GFP (PaGFP) tagged desmocollin 2a (Dsc2a), plakoglobin (PG) and plakophilin 2a (Pkp2a). Cells were cultured for 1 d before recordings. Images are presented in a colour intensity scale. Dashed boxes indicate ROI before photoactivation; scale bar: 5 μm. (B) Mean FLAP mobile fraction of Dsc2a, PG and Pkp2a. The box represents the 25-75th percentiles, and the median

is indicated in red. The whiskers show the range of values. ***P ≤ 0.001 (student's t-test). (C) Representative time-lapse images showing photoactivation of Dsc2a-PaGFP (green; mScarlet-Pkp2a in magenta) in comparison to PaGFP-Pkp2a (green; Dsc2a-mScarlet in magenta) stably expressed in MDCK cells over a 30 min period. Dashed boxes indicate ROI before photoactivation; scale bar: 10 µm. (D) Cytoplasmic photoactivation of PaGFP-Pkp2a (green; Dsc2a-mScarlet in magenta) stably expressed in MDCK cells. 10 µm circle indicates photoactivated ROI at 0s; dotted lines indicate the outline of the cell; scale bar: 10 µm. (E) Fluorescence intensity of PaGFP-Pkp2a over time showing the rapid decrease in photoactivated cytoplasmic ROIs concomitant signal increase at the membrane (n=5 cells per experiment, N=3; error bars are ±s.e.m.) (F) Line profile plots showing overlapping peaks of fluorescence signal of PaGFP-Pkp2a and Dsc2a-mScarlet after 5 min indicated by the box in (D).

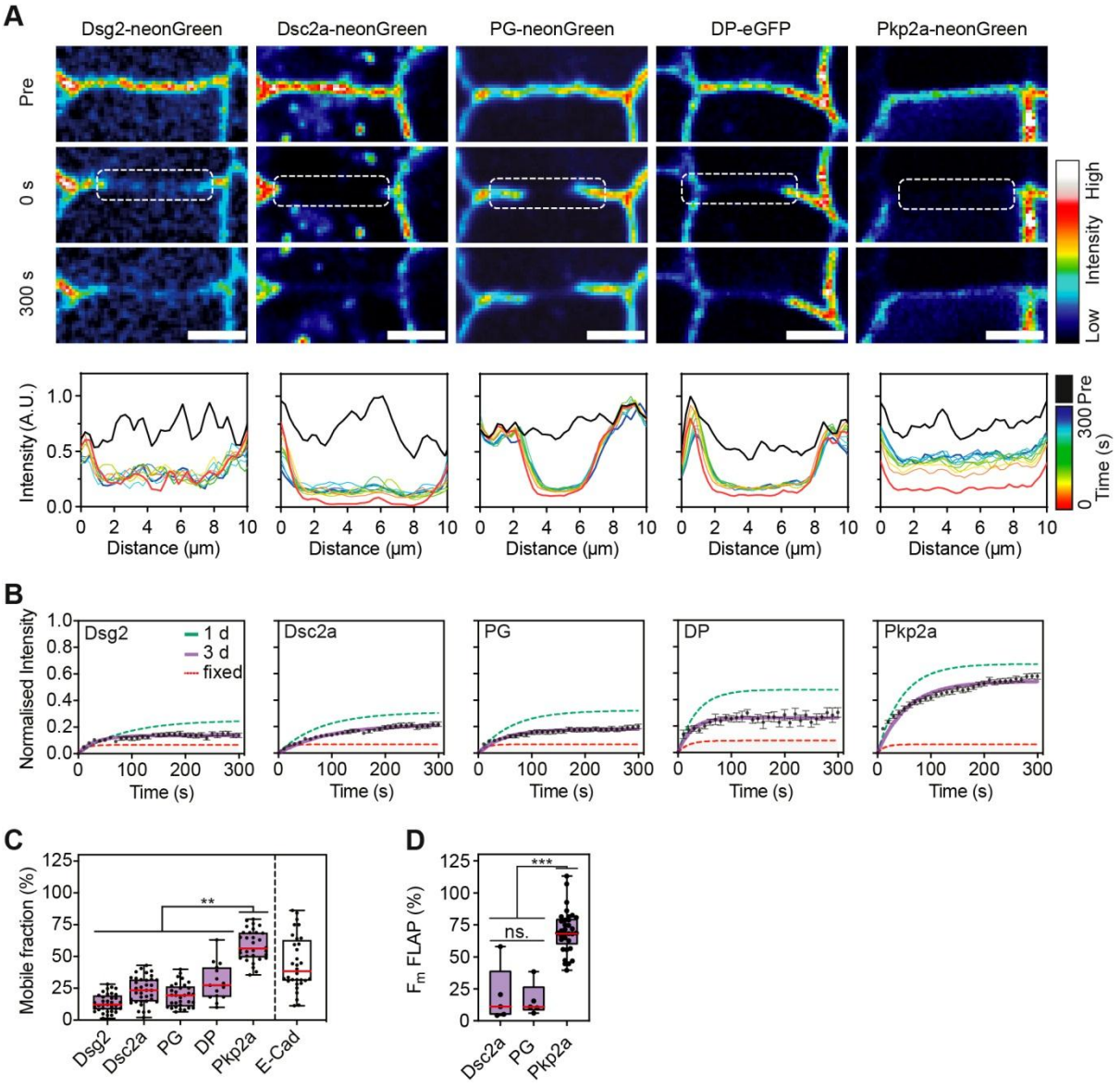

Figure 3. Protein dynamics are reduced but Pkp2a remains significantly more mobile in hyper-adhesive desmosomes. (A) Representative time-lapse images showing FRAP in MDCK cells transfected with neonGreen-labelled desmoglein 2 (Dsg2), desmocollin 2a (Dsc2a), plakoglobin (PG) and plakophilin 2a (Pkp2a), and eGFP tagged Desmoplakin (DP). The cells were cultured confluent for 3 d leading to the acquisition of hyper-adhesion in the majority of desmosomes. Images are presented in a colour intensity scale. Graphs show the line profile plots of the bleached ROIs (dashed box at 0s) over time in a colour intensity scale. Scale bar: 5 µm. (B) Graphs show the mean fluorescence recovery curves for all recorded desmosomes in 3 d monocultures (n=15-42 error bars are ±s.e.m.); dashed green line indicates mean recovery curve in 1 d monocultures; red line showing the

recovery of PFA-fixed samples (reversible photobleaching). (C) FRAP mean mobile fraction values for the indicated desmosomal proteins in 3 d monolayers (scatter plot). (n=15-42, N=3). (D) FLAP mean mobile fractions of Dsc2a-PaGFP, PG-PaGFP and PaGFP-Pkp2a comparing 1d or 3d cultured monolayers. The box represents the 25-75th percentiles, and the median is indicated in red. The whiskers show the range of values. ns. no significant difference; *P<0.05; **P<0.01; ***P<0.001 (Kruskal-Wallis with Dunn's multiple comparisons test).

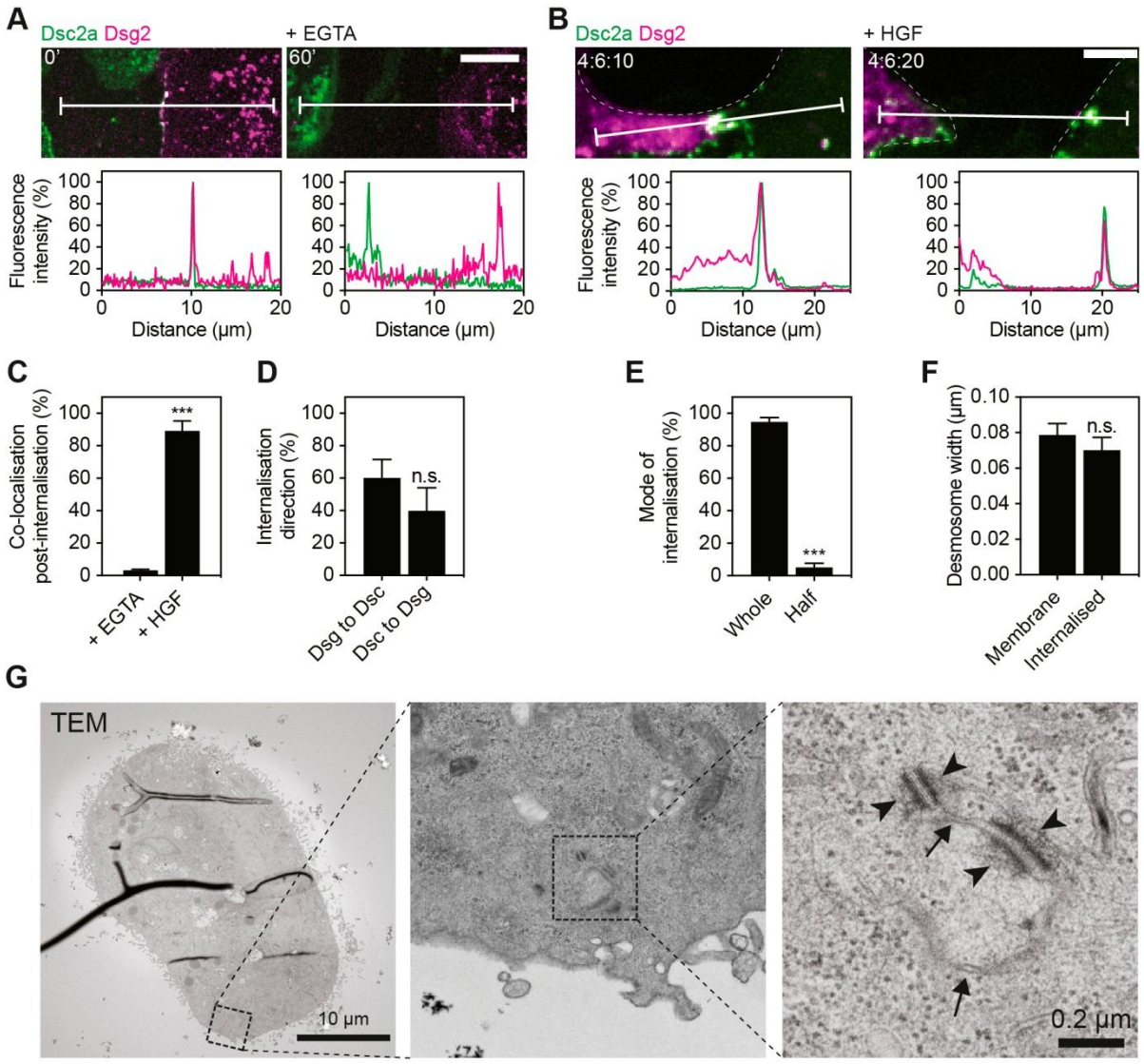

Figure. 4. Hepatocyte growth factor-induced cell scattering leads to whole desmosome internalisation. (A) Mixed populations of MDCK cells expressing either desmocollin 2a tagged with YFP (Dsc2a, green) or desmoglein 2 tagged with mCherry (Dsg2, magenta) were cultured for 1 d before calcium chelation with EGTA (3 mM) for 60 min. Scale bar: 5 μm. Fluorescence line profiles depict the fluorescence intensity along the white line in the images. Desmosomes are indicated by the co-localisation of the fluorescence signals. Note the separate internalisation of Dsc2-YFP and Dsg2-mCherry by the adjacent cells. (B) Treatment with hepatocyte growth factor (HGF, 40 ng/ml) for 4 h induced scattering of MDCK cells and lead to the joined internalisation of both Dsc2a-YFP and Dsg2-mCherry by one or the other of the adjacent cells. Cells were cultured subconfluent and serum starved for 12 h before HGF treatment. Dotted lines indicate the outline of the cells; scale bar: 5 μm.

Fluorescence line profiles depict the fluorescence intensity along the white line in the images. (C) Quantification of co-localisation of Dsc2a-YFP and Dsg2-mCherry after internalisation induced by 90 min Ca^{2+} chelation or 6 h HGF treatment. (EGF n=252 desmosomes, N=3; HGF n=121 desmosomes, N=18, mean±s.e.m) (D) Quantification of internalisation direction either Dsg2-mCherry into the Dsc2a-YFP expressing cell or vice versa following 6 h HGF treatment. (n=108 desmosomes, N=18, mean±s.e.m) (E) Analysis of the mode of desmosome internalisation, either whole or half, revealed by transmission electron microscopy (TEM) following 6 h HGF treatment. (n=30 cells, N=3, mean±s.e.m) (F) Graph showing the plaque-to-plaque width of the desmosomes measured on TEM images remains mostly unchanged after internalisation. (n = 10 desmosomes/cell of 10 cells/group, N=3, mean±s.e.m) (G) Representative TEM images of internalised double membrane structures (arrows) with intact whole desmosomes with attached intermediate filament fragments on each side of the doublet (arrowheads). ***P<0.001; n.s. no significant difference (student's t-test).

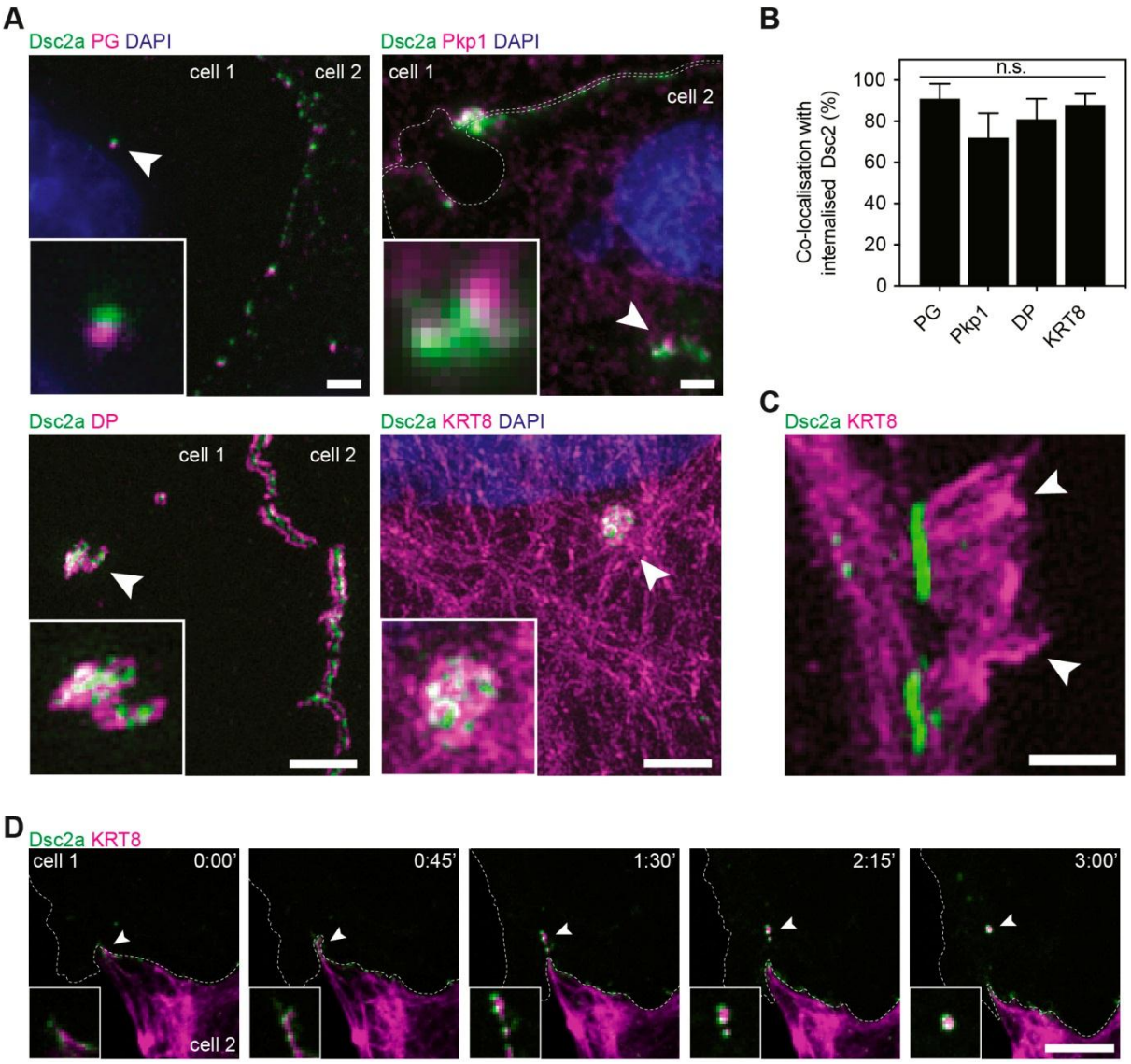

Figure 5. Internalised whole desmosomes are composed of all major desmosomal and keratin fragments. (A) MDCK cells stably expressing desmocollin 2a tagged with YFP (Dsc2a) were induced to scatter by hepatocyte growth factor (HGF, 40 ng/ml) treatment. Cells were immunostained for plakoglobin (PG), plakophilin 1 (Pkp1), desmoplakin (DP) and keratin filaments (KRT8). Representative structured illumination microscopy (SIM) images. Arrows indicate internalised desmosomes, dotted lines indicate the outline of the cell; scale bar: 5 µm. (B) Quantification of the co-localisation of internalised Dsc2a-YFP with the respective protein. (n=64-165 desmosomes, N=3, mean±s.e.m); n.s. no significant difference (Kruskal-Wallis with Dunn's multiple comparisons test). (C) Representative SIM image showing fragments of keratin filaments attached to internalised desmosomes. Arrows indicate severed keratin filaments; scale bar: 1

μm. (D) Time-lapse images showing co-internalisation of keratin 8 (KRT8) with desmosomes in scattering cells. MDCK cells stably expressing Dsc2a-YFP (green, cell 1) were transiently transfected with keratin 8 tagged with mCherry (KRT8, magenta, cell 2) and treated with HGF (40 ng/ml) for 4 h. Images every 45 sec shown; arrows indicated internalised desmosomes with keratin filaments; dotted lines indicate the outline of the cell; scale bar: 5 μm.

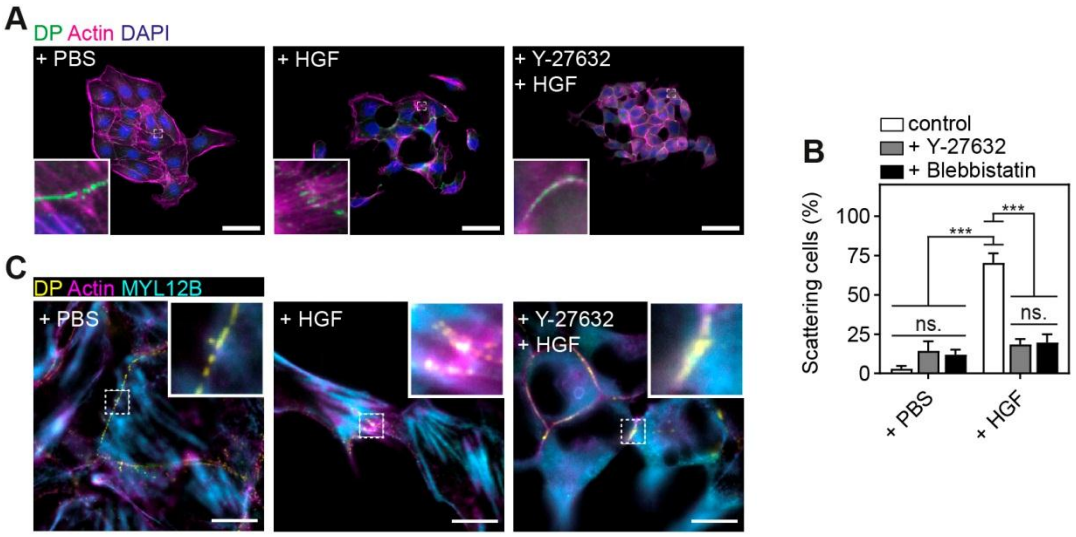

Figure 6. Hepatocyte growth factor induced cell scattering is actomyosin dependent. (A) Representative images showing MDCK wt cells stained for desmosomes with α-desmoplakin (DP, green), actin with phalloidin (magenta) and cell nucleus with DAPI (blue). Cells were treated with PBS as control, hepatocyte growth factor (HGF, 40 ng/ml) for 6 h or pre-treated for 1 hour with Y-27632 (50 µM), followed by co-treatment with HGF and the inhibitor for 6 h. Scale bar: 50 µm. Note the increase of stress fibres at sites of desmosomes in HGF-treated cells before internalisation and the lack thereof when treated with Y-27632. (B) Quantification of scattering cells, which only remained attached to two neighbouring cells in proportion to the total cell number of the cell islet. Cells were treated with PBS, Y-27632 (50 µM) or blebbistatin (50 µM) for 1 h. To induce scattering cells were treated with HGF (40 ng/ml) for 6 h or pre-treated for 1 hour with Y-27632 (50 µM), followed by co-treatment with HGF and the inhibitor for 6 h. (n=91-315 cells, N=3, mean±s.e.m); ***P<0.001; n.s. no significant difference (Kruskal-Wallis with Dunn's multiple comparisons test). (C) Representative images of cells treated like in (A) but co-stained for DP (yellow), actin (magenta) and myosin regulatory light chain (MYL12B, cyan). Scale bar: 10 µm.

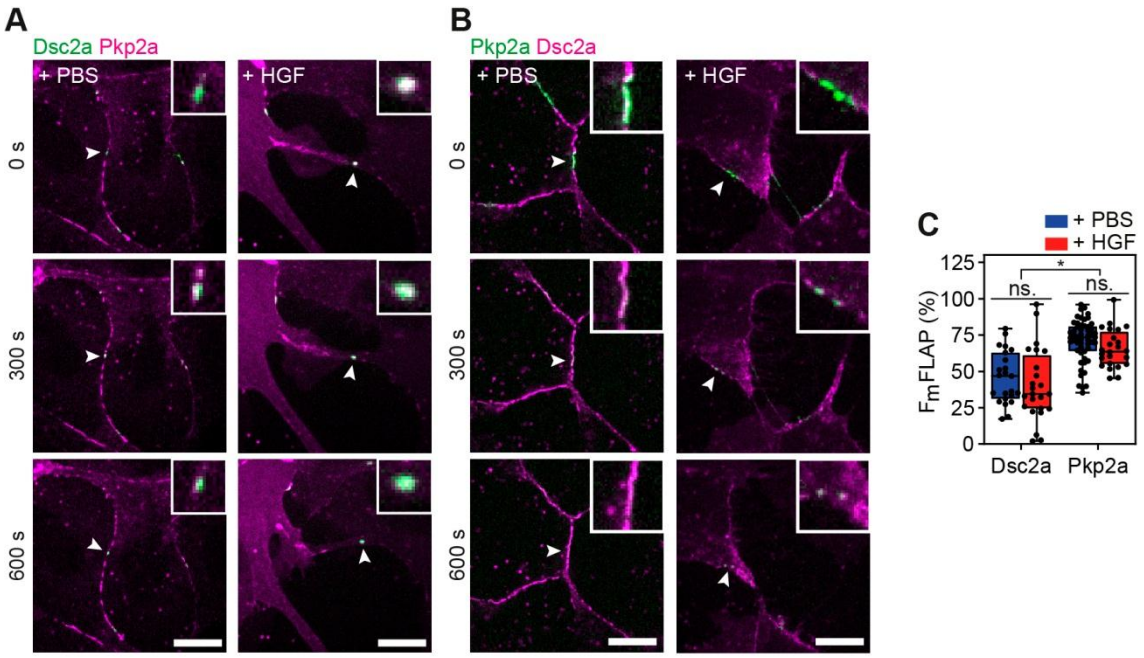

Figure 7. The mobility of desmosomal proteins remains unchanged following internalisation. (A) Representative time-lapse images showing FLAP in MDCK cells stably expressing desmocollin2a tagged with PaGFP (Dsc2a, green) and plakophilin 2a tagged with mScarlet (Pkp2a, magenta). Cells were cultured subconfluent, serum starved for 12 h and treated for 4 h with hepatocyte growth factor (HGF, 40 ng/ml) or same v/v PBS as control. (B) In comparison to (A) MDCK cells were transfected with PaGFP-Pkp2a (green) and Dsc2a-mScarlet (magenta). Arrows indicate photoactivated ROI enlarged in the inserts; scale bar: 10 µm. (C) Mean FLAP mobile fraction values of Dsc2a and Pkp2a comparing PBS control and HGF treated cells (scatter plot). (n=23-53, N=3). The box represents the 25-75th percentiles, and the median is indicated in red. The whiskers show the range of values. ns. no significant difference; *P<0.05 (Kruskal-Wallis with Dunn's multiple comparisons test).

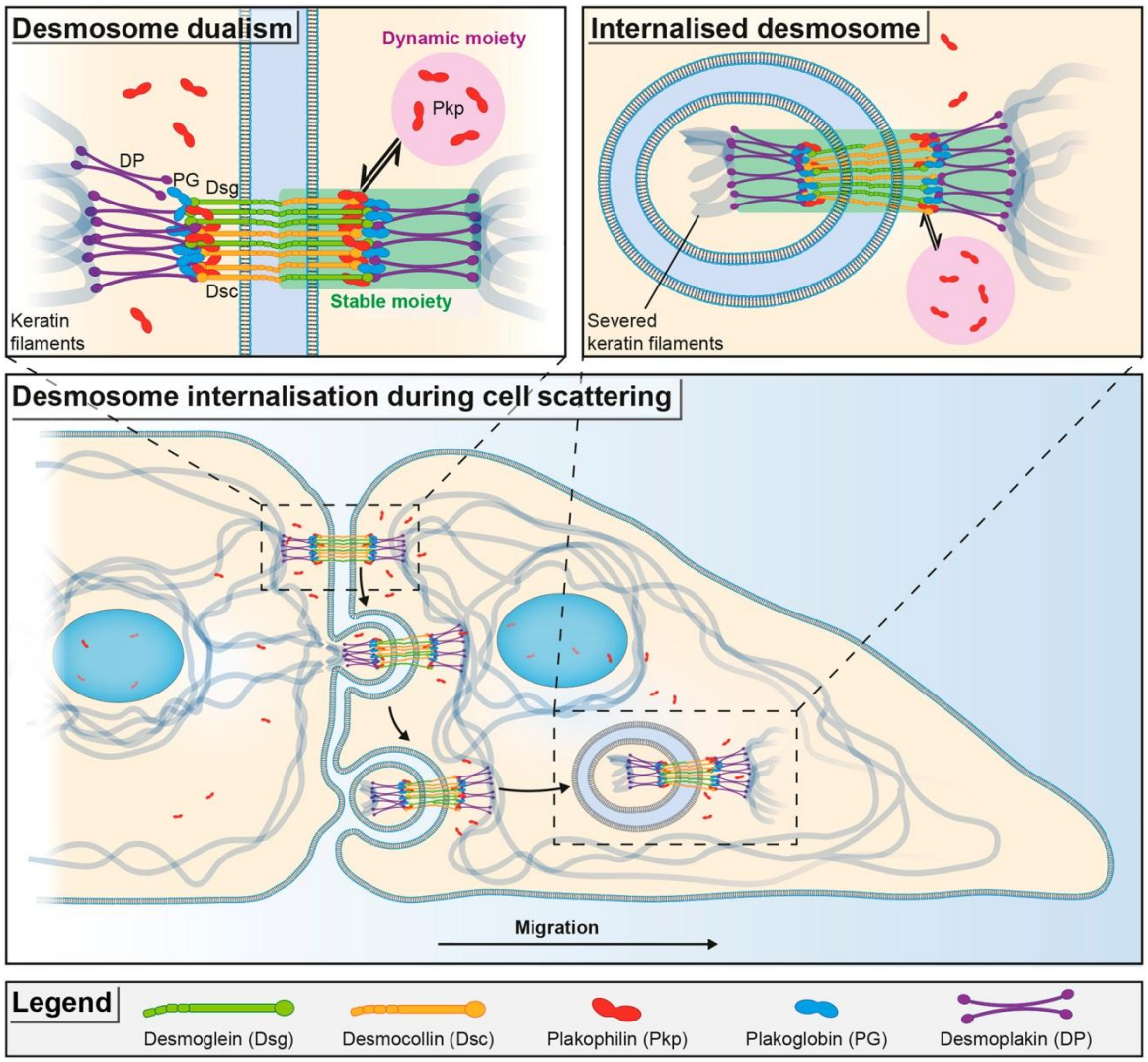

Figure 8. Model of desmosome dualism and desmosome internalisation during growth factor-induced cell scattering. Desmosomes consist of two contrasting protein moieties or modules, a strikingly stable moiety (shaded in green), composed of desmocollins and desmogleins (the desmosomal cadherins), plakoglobin and desmoplakin, and a high mobility moiety (shaded in magenta), represented by plakophilin 2a (Pkp2a). As desmosomes mature from calcium-dependence to calcium-independent hyper-adhesion, their stability increases, but Pkp2a remains highly mobile. Desmosome down-regulation during growth factor-induced cell scattering proceeds by internalisation of the whole desmosomal complex including attached keratin filaments by one of the pair of adjacent cells. The internalised complex retains a stable moiety and highly mobile Pkp2a.

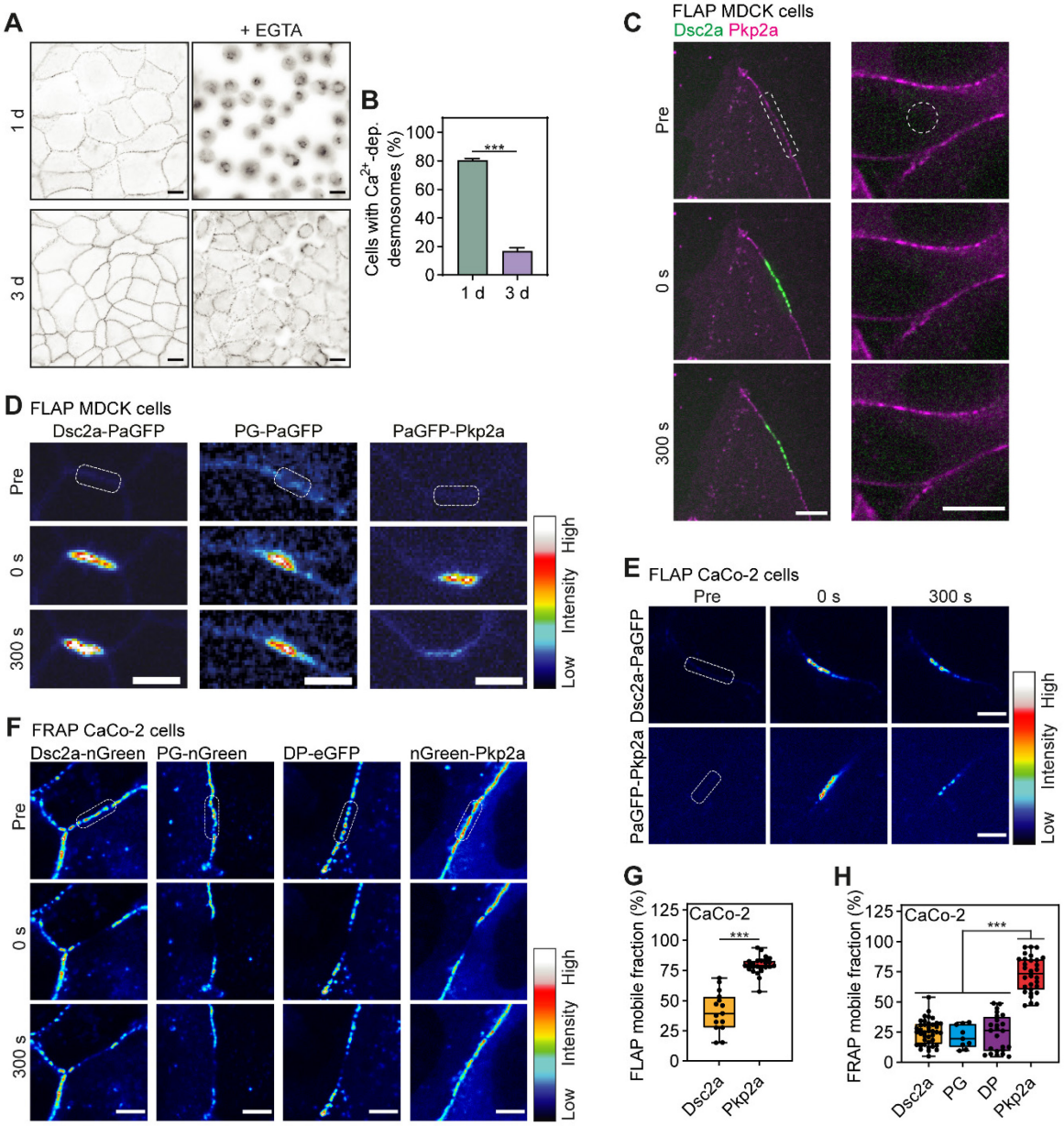

Fig. S1. Differential desmosomal protein dynamics depend on spatial and temporal conditions, but their dualistic composition is independent of the cell type. (A) Representative images of MDCK wt cells acquiring calcium-independence. The cells were cultured confluent for 1 or 3 d, treated Ca^{2+}-chelating medium (+ EGTA, right panel) for 90 min and stained for desmoplakin. Left panel untreated control cells. Scale bar: 10 µm. (B) Quantification of MDCK cells with calcium-dependent desmosomes. Pooled data from all MDCK cell lines used in this study. (1d n=69; 3d n=46; ≥5 measurements per cell line; N=3). (C) Representative time-lapse images showing FLAP in MDCK cells stably expressing desmocollin 2a (Dsc2a, green) tagged with photoactivatable GFP (PaGFP) and plakophilin 2a (Pkp2a, magenta) tagged with mScarlet. Cellts were cultured for 1d. Dashed overlay indicates ROI before photoactivation either at the membrane or in the cytoplasm. Note to absence of a cytoplasmic pool of Dsc2a. Scale bars: 10 µm. (D) Representative time-lapse images comparing FLAP in MDCK cells stably expressing either PaGFP tagged Dsc2a, plakoglobin (PG) or Pkp2a after 3 days of confluent culturing. Images are presented in a colour intensity scale; dashed box indicated ROI before photoactivation; scale bar: 5 µm. Note the significant loss of fluorescence of PaGFP-Pkp2a in comparison to Dsc2a-PaGFP and PG-PaGFP. (E) Representative time-lapse images of FLAP of 1 d cultured CaCo-2 cells transiently transfected with Dsc2a-PaGFP or PaGFP-Pkp2a. Images are presented in a colour intensity scale; dashed box indicated ROI before photoactivation; scale bar: 5 µm. (F) Representative time-lapse images of FRAP of 1 d cultured CaCo-2 cells transiently transfected with neonGreen-labelled Dsc2a, PG and Pkp2a, and eGFP tagged DP. Images are presented in a colour intensity scale; dashed box indicated ROI before bleaching; scales bar: 5 µm. (G) Mean FLAP mobile fraction of Dsc2a and Pkp2a in CaCo-2 cells (scatter plot). n=15-25, N=3. ***P<0.001; (student's t-test). (H) Mean FRAP mobile fraction of the indicated desmosomal proteins in CaCo-2 cells (scatter plot). n=9-40, N=3. ***P<0.001; (Kruskal-Wallis with Dunn's multiple comparisons test). The box of the scatter plots represents the 25-75th percentiles, and the median is indicated in red. The whiskers show the range of values.

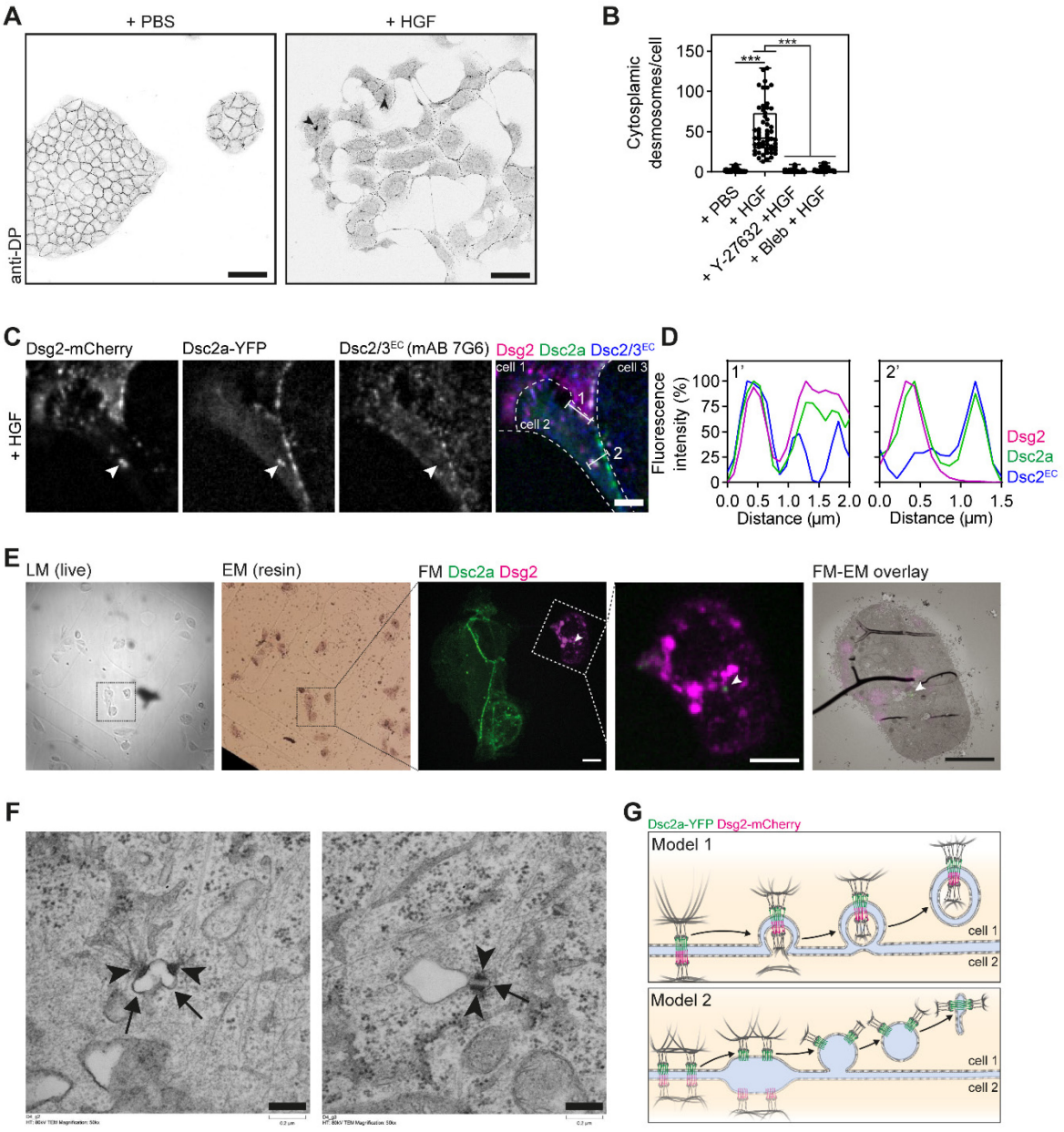

Fig. S2. Hepatocyte growth factor-induced cells scattering leads to whole desmosome internalisation and is dependent on actomyosin. (A) Representative images of hepatocyte growth factor (HGF) - induced cell scattering of MDCK cells. Cells were cultured sub-confluent for 2 d, serum-starved for 12 h, treated for 4 h with 40 ng/ml HGF or same v/v PBS as control, and stained for desmoplakin (DP). Arrows indicate clustering of internalised desmosomes, scale bars: 50 µm. (B) Quantification of internalised desmoplakin positive particles (cytoplasmic desmosomes) with a minimum size of 20 nm^2 in the cytoplasm 2 µm peripheral of the membrane. MDCK cells were with PBS as a control, with HGF (40 ng/ml) for 6 h or pre-treated for 1 hour with Y-27632 (50 µM), followed by co-treatment with HGF and the inhibitor for 6 h. ***P<0.001; (Kruskal-Wallis with Dunn's multiple comparisons test). (C) Representative images of mixed populations of MDCK cells expressing either desmocollin 2a tagged with YFP (Dsc2a-YFP) or desmoglein 2 tagged with mCherry (Dsg2-mCherry) immunostained with a specific antibody against the extracellular domain of Dsc2/3, following 6 h of HGF treatment (40 ng/ml). Cells were unpermeabilsed before staining. Arrow indicates internalised desmosomes. Dotted lines indicate outlines of the cells, scale bar: 2 µm. (D) Fluorescence line profiles depicting the fluorescence intensity along the white lines in (C). Note the co-localisation of the antibody (blue) with Dsc2a-YFP (green) and Dsg2-mCherry (magenta) at the membrane and no co-localisation with the internalised desmosome in 2'. (E) Representation of for correlative light and electron microscopy to identify cells which had internalised double-labelled desmosomes. Mixed populations of MDCK cells expressing either Dsc2a-YFP (green) or Dsg2-mCherry (magenta) were used. LM = light microscopy, EM = electron microscopy, FM = fluorescent microscopy. Arrow indicates double-labeled internalised desmosomes; scale bars: 10 µm. (F) Representative transmission electron microscopy images of internalised half-desmosomes (arrowheads) with single membrane structures (arrows). Scale bars: 0.2 µm. (G) Alternative models illustrating the internalisation of desmosomes following HGF-induced cell scattering. Model 1 depicts the dominant way in which desmosomes are internalised based on co-localisation and EM data, whereas Model 2 may illustrate the rare instances when half-desmosomes are internalised and neighbouring desmosomes coalesce as seen in (F).

Table S1. Desmosome dynamics in MDCK cells change after acquisition of hyper-adhesion.

	Post-confluent time (d)	Mobile fraction (%)	$t_{1/2}$ (s)
Desmoglein 2 [1]			
	1	30 ± 3	76 ± 7
	3	14 ± 1 ****	N/D
Desmocollin 2a [1]			
	1	36 ± 2	63 ± 6
	3	23 ± 2 ****	67 ± 8 ns.
Plakoglobin [1]			
	1	38 ± 3	69 ± 6
	3	20 ± 2 ****	N/D
Desmoplakin I [2]			
	1	50 ± 4	N/D
	3	30 ± 4 **	N/D
Plakophilin 2a [1]			
	1	75 ± 2	30 ± 2
	3	59 ± 2 ****	45 ± 4 **
E-cadherin			
	1	53 ±4	46 ± 6
	3	45 ±4 ns.	40 ± 6 ns.
[1]neonGreen	N/A	7±1	11±3
[2]eGFP	N/A	10±2	13±3

Protein dynamics of confluent monolayers of MDCK cells measured using FRAP. All measurements represent means of all independent measurements of N=3 experiments. ****P<0.0001; **P<0.01; ns. no significant difference; versus 1 d monolayers (student's t-test). The mobile fractions of the proteins present a reliable readout of the protein dynamics. The fast $t_{1/2}$ of the fluorophores (reversible photobleaching) impaired the determination accurate $t_{1/2}$ in particular regarding the eGFP-tagged desmoplakin and the highly stable neonGreen-tagged desmoglein 2 and plakoglobin in hyper-adhesive desmosomes (3 d); N/D, not determined.

Table S2. Vectors and primers used to clone tagged constructs.

Constructs	Restriction Enzymes	Primers used to obtain PCR fragments
pDsc2a-PaGFP	BamHI/NheI	FOR. GTCAGCTGACGCGTGCTAGCATGGTGAGCAAGGGCGAG REV. TGTAGAGAAAAATTTCTTATGACTCTTACTTGTACAGCTCGTCCATGCCGAG
pDsc2a-neonGreen	BamHI/NheI	FOR. GTCAGCTGACGCGTGCTAGCATGGTGAGCAAGGGCGAGGAGGA REV. TGTAGAGAAAAATTTCTTATGACTCTTAGACACCATGGTGGCGAC
pDsc2a-mScarlet	BamHI/NheI	FOR. GTCAGCTGACGCGTGCTAGCATGGTGAGCAAGGGCGAG REV. TGTAGAGAAAAATTTCTTATGACTCTTATCTAGATCCGGTGGATCCCGG
pDsg2-PaGFP	NcoI only	FOR. AAAGGAGGTACCCACGCCACATGGCGCGGAGCCC REV. AGCTCCTCGCCCTTGCTCACGGAGTAAGAATGCTGTACAGTGCTATG
pDsg2-neonGreen	HindIII only	FOR. CCCGCCAGCGGCCGCTGCCAAGCTTATGGCGCGGAGCCC REV. TTTGAATTCGAGAGCTCGGAAGGAGTAAGAATGCTGTACAGTGCT
pPaGFP-PG	XbaI/EcoRI	FOR. CCACACCCAAGCTGTATGGTGAGCAAGGGCGAG REV. AGTCCAGTGTGGTGGAATTCCTTGTACAGCTCGTCCATGCC
pneonGreen-PG	XbaI/EcoRI	FOR. CCACACCCAAGCTGTATGGTGAGCAAGGGCGAGGAGG REV. AGTCCAGTGTGGTGGAATTCCTTGTACAGCTCGTCCATGC
pPaGFP-Pkp2a	EcoRI/EcoRV	FOR. CACACCCGCCAGCGGCCGCTGCCAAGCTTCCGAGCTCTCGATGGTGAGCAAGGGCG REV. GGGCGCCGGGGGCTGCCATTCTAGAAACCTCGAGGTAGATCTTGTACAGCTCGTCCATGCC
pneonGreen-Pkp2a	XbaI/EcoRI	FOR. CCACACCCAAGCTGTATGGTGAGCAAGGGCGAGGAGG REV. AGTCCAGTGTGGTGGAATTCCTTGTACAGCTCGTCCATGC
pmScarlet-Pkp2a	EcoRI/EcoRV	FOR. CACACCCGCCAGCGGCCGCTGCCAAGCTTCCGAGCTCTCGATGGTGAGCAAGGGCG REV. ATCGATTGTATCAGTCAGTCAGTGCAGGAGGAGACAACTTCTAGATCAGTCTTTAAGGGAGTGGTAGGC

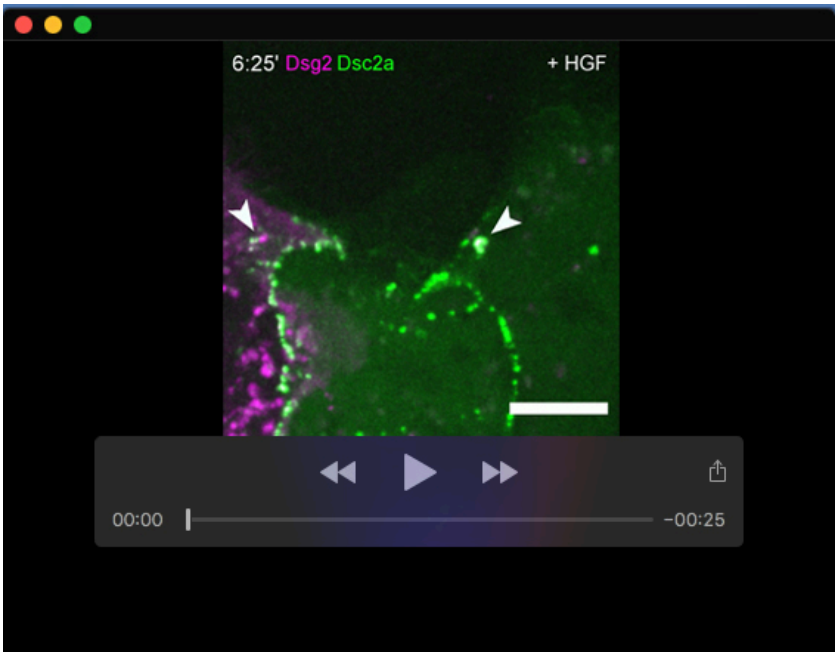

Movie 1. Related to Figure 4. Recording of whole desmosome internalisation of HGF-treated MDCK cells expressing the indicated desmosomal proteins.

Time-lapse confocal microscopy movie of scattering MDCK cells expressing either Desmocollin tagged with YFP (Dsc2a, green) or Desmoglein 2 tagged with mCherry (Dsg2, magenta). Images were acquired every 5 sec for 10 min (internalisation shown), starting after 4h after addition of HGF (40 ng/ml). Scale bar indicates 5 µm. Arrows indicate double-labeled desmosome (white).

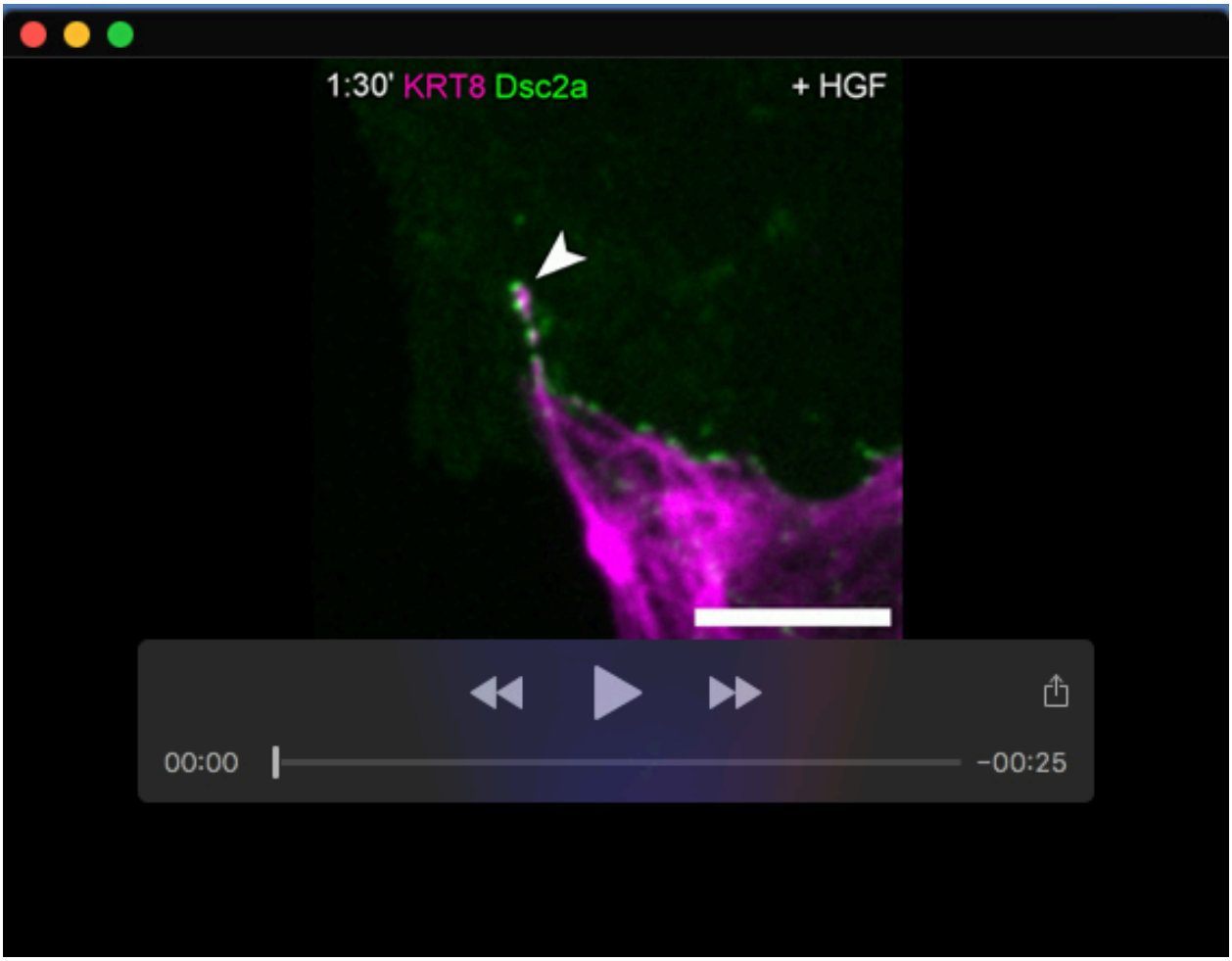

Movie 2. Related to Figure 5. Recording of co-internalisation of keratin filaments with whole desmosomes of HGF-treated MDCK cells.

Time-lapse confocal microscopy movie of scattering MDCK cells expressing either Desmocollin 2a tagged with YFP (Dsc2a, green) or keratin 8 tagged with mCherry (KRT8, magenta). Images were acquired every 15 sec for 7 min, starting after 4 h after addition of HGF (40 ng/ml). Scale bar indicates 5 µm. Arrows indicate internalised desmosomes with keratin filaments from the adjacent cell.

Journal of Cell Science • Supplementary information